Peer reviewed version

Link to published version (if available):
10.1016/j.chemgeo.2018.09.024

Link to publication record in Explore Bristol Research
PDF-document

University of Bristol - Explore Bristol Research
General rights

Accepted Manuscript

The effects of lithology on trace element and REE behavior during tropical weathering

María Chapela Lara, Heather L. Buss, Julie C. Pett-Ridge

The effects of lithology on trace element and REE behavior during tropical weathering

María Chapela Lara [1,2,*], Heather L. Buss [2], Julie C. Pett-Ridge [3]

[1] Department of Natural Resources and the Environment, University of New Hampshire, James Hall, Durham, New Hampshire, 03824, USA.

[2] School of Earth Sciences, University of Bristol, Wills Memorial Building, Bristol, BS8 1RJ, UK.

[3] Department of Crop and Soil Sciences, Oregon State University, Corvallis, Oregon, 97330, USA.

*Corresponding author: glzmcl@my.bristol.ac.uk

Abstract

The thick regolith developed in the humid tropics represents an endmember of critical zone evolution, where shallow and deep biogeochemical cycles can be decoupled in terms of the predominant source of trace elements (atmospheric input at the surface, weathering at depth) and of the processes that control their cycling. To investigate the influence of lithology on trace element behavior and in this potential decoupling, we studied two deep (9.3 and 7.5 m), highly-leached, ridgetop regolith profiles at the Luquillo Critical Zone Observatory, Puerto Rico. These profiles have comparable internal (degree of weathering, topography) and external (vegetation, climate) characteristics, but differ in their underlying bedrock (andesitic volcaniclastic and granitic). At these two sites, we analyzed a large suite of trace elements and used the rare earth elements and yttrium (REY) as tracers of critical zone processes because they are fractionated by the chemical reactions involved in weathering and pedogenesis (e.g., sorption, dissolution, colloidal transport) and by redox fluctuations.

We found that both regolith profiles show atmospheric inputs of trace elements at the surface and evidence of bedrock dissolution at depth, as expected. We also found noticeable differences in the re-distribution of trace elements and REY within the profiles, indicative of different geochemical environments with depth and lithology. In the volcaniclastic profile, trace element and REY behavior is controlled mainly by redox-mediated, sorption/desorption reactions, whereas pH-controlled dissolution/precipitation and sorption reactions predominate in the granitic profile. The most noticeable difference between the two regolith profiles is in the long-term redox conditions, inferred from redox-sensitive elements and Ce anomaly variations, which are more variable and stratified in the volcaniclastic profile and change gradually with depth in the granitic profile. The contrasting redox conditions and the different sources of elements (dust vs. bedrock) produce a decoupling between the surface and deep geochemical environments of the volcaniclastic regolith. The difference in redox conditions between the two lithologies likely stems from the finer grain size and higher clay content of the volcaniclastic regolith.

Keywords: Rare earth elements, REE, REY, trace elements, redox conditions, tropical weathering, mass transfer, critical zone.

1. INTRODUCTION

Chemical elements are released from minerals during weathering and then retained in soils or drained into streams, at rates modulated by critical zone processes. Processes occurring anywhere within a regolith profile can contribute to these critical zone modulating functions, but certain regions may have proportionally larger roles. One of these 'hot spots' is the saprolite to soil transition, that delimits the shallow, well-aerated, biologically driven soil and the deep, weathering and transport-controlled saprolite. Deep regolith may also be decoupled from the surface in terms of the predominant source of nutrients to the biota: atmospheric inputs and vegetation recycling in the

upper domain and bedrock weathering and leaching of nutrients in the lower domain (e.g., Bruijnzeel, 1991; Buss et al., 2005). These differences in the sources of elements and in the processes controlling their mobilization, transformation and redistribution may also underlie the ecological functioning of different zones of the regolith, manifested in its most extreme in the humid tropics, where regolith tens of meters deep develops on geomorphically stable areas such as ridgetops (e.g., Braun et al., 2012; Butt et al., 2000; Hewawasam et al., 2013; Pope, 2013; Porder and Hilley, 2011; Teng et al., 2010).

Chemical weathering of bedrock is a primary source of mineral nutrients to regolith and parent lithology also influences the dynamics of nutrients through fundamental controls on various geochemical, biological and physical processes (e.g., De Kimpe et al., 1984; Fritz, 1988; Navarre-Sitchler et al., 2015). For example, in the Luquillo Critical Zone Observatory (LCZO), regolith overlying volcaniclastic bedrock is thicker than regolith overlying granitic bedrock (Buss et al., 2017; Fletcher and Brantley, 2010), reflecting its approximately seven times faster weathering rate (Dosseto et al., 2012) and its lower susceptibility to landslides (Larsen, 2012). Another example is the different fracturing style of these two bedrocks (blocky in the volcaniclastic vs. spheroidal in the granitic; Buss and White, 2012), which in turn affects permeability, mineral dissolution rates, the spatial distribution of mineral nutrients and other elements, groundwater flow, topography, runoff and nutrient export fluxes (e.g., Buss et al., 2017; Porder et al., 2015; Stallard, 2012). However, at the advanced stages of weathering represented by thick tropical regolith, the influence of lithology on shallow critical zone processes and biogeochemical cycles is expected to decrease (Porder, 2014), while atmospheric inputs (dust, sea spray and rainfall) become more important (e.g., Clergue et al., 2015; Chadwick et al., 1999; Derry and Chadwick, 2007; Viers and Wasserburg, 2004).

The relative importance of the different sources of mineral nutrients and of the processes that determine their re-distribution within the critical zone, can be interpreted by examining the concentrations of trace elements in regolith depth profiles, including rooting-zone soil and the

deeper weathered material such as saprolite that overlies intact bedrock (Brantley and Lebedeva, 2011; Brantley and White, 2009). However, while several studies have examined the behavior of trace elements in thick regolith (e.g., Braun et al., 1990, 1998; Jiang et al., 2018; Ma et al., 2007), little is known about the specific influence of lithology independent of other factors like climate, vegetation and topography.

To trace the inputs, losses and translocations of elements within regolith profiles, we can use the fact that certain elements remain behind as others are solubilized and removed during chemical weathering (e.g., Ebelmen, 1845; Merrill, 1906; Chadwick et al., 1990; Brantley and Lebedeva, 2011). The elements that remain in the regolith, such as Zr, Ti and Nb, are mostly hosted in minerals that are resistant to weathering and thus can be considered immobile in many circumstances (e.g., Brimhall and Dietrich, 1987; Harden, 1982; Nesbitt and Markovics, 1997), although Ti and Zr can be mobile in tropical regolith (Braun et al., 1993, 2005; Buss et al., 2017; Kurtz et al., 2000; Ma et al., 2007; Nahon and Merino, 1997). Other elements, like Al and Fe, are poorly soluble and form secondary minerals and thus are also largely retained in the regolith. In contrast, alkali, alkaline-earth (e.g., Nesbitt and Markovics, 1997; Nesbitt and Young, 1982) and rare earth elements are easily removed from primary minerals, with stocks generally decreasing with increasing weathering intensity (e.g., Banfield and Eggleton, 1989; Jin et al., 2017).

The rare earth elements (REE) have very similar chemical and physical properties (Laveuf and Cornu, 2009) and therefore behave similarly in the environment (Henderson, 1984; Tyler, 2004). However, their properties vary slightly along the series (e.g., decreasing ionic radius, increasing ionic potential and increasing electronegativity from La to Yb; Laveuf and Cornu, 2009), making them useful tracers of biogeochemical processes in low temperature systems (e.g., Bau and Koschinsky, 2009; Elderfield et al., 1990; Vázquez-Ortega et al., 2015). Rare earth elements are usually grouped into two or three categories. 1) Light REE (LREE) have a mean atomic mass of <153 and an effective radius of > 95 pm (La, Ce, Pr, Nd, Sm and Eu). 2) Heavy REE (HREE) have

a mean atomic mass of >153 and effective ionic radius of < 95 pm (Gd, Tb, Dy, Ho, Er, Tm, Yb and Lu), with yttrium often included in this group due to its small ionic radius. 3) Medium REE (MREE), loosely designate REE with intermediate mean atomic mass and ionic radii and can include Eu, Gd, Tb and Dy.

The distribution of REE and yttrium (REY) during weathering reflects their relative mobilities, controlled by the formation of aqueous complexes and pH-controlled sorption/desorption and co-precipitation reactions (Byrne and Li, 1995; Devranche et al., 2005; Henderson, 1984; Laveuf and Cornu, 2009; Pourret et al., 2007; Sholkovitz, 1995), especially with Fe, Mn- and Al-(hydr)oxides (Bau, 1999; Bau and Koschinsky, 2009). REY are also fractionated by a number of mechanisms related to the redox conditions of their environment. For example, fluctuations in the Eh of natural soils that result from wetting-drying events and rapid microbial responses can mobilize REY, through colloidal dispersion of nano-particles enriched in REY (Braun et al., 1998; Thompson et al., 2013; Viers et al., 1997).

Redox conditions can also directly fractionate REY that have more than one valence state. Notably, Ce can be trivalent, like the majority of REE, or tetravalent under oxidizing conditions. Trivalent Ce is oxidized to Ce (IV) at Eh values of ~0.3 V (De Carlo et al., 1998), a common condition in sub-oxic to oxic surficial environments like soils. The oxidation of Ce induces changes in charge and ionic radius that decouple it from the rest of the REE, allowing its incorporation into secondary solid phases (Laveuf and Cornu, 2009). Tetravalent Ce is also adsorbed more strongly than the other, trivalent REE (Devranche et al., 2005). Moreover, if soluble Ce^{3+} is oxidized to Ce^{4+}, it can precipitate as very insoluble cerianite (CeO_2). This suite of Ce oxidation, scavenging and precipitation reactions can result in solids exhibiting a positive Ce anomaly. Indeed, although the geochemistry of Ce is scarcely documented in the critical zone, with most studies based on marine environments, positive Ce-anomalies have been found in regolith profiles on various parent lithologies (Braun et al., 1998; Ma et al., 2007; Vázquez-Ortega et al., 2015, 2016). Conversely,

Ce^{4+} is more likely to be mobilized under anoxic conditions, leading to a depletion in Ce relative to oxic conditions.

The properties of different bedrock types, such as primary mineralogy and grain size, may contribute to different permeabilities, promoting different local redox conditions, which in turn will determine the weathering and transport processes that control trace element production and speciation. Many redox-sensitive elements are micronutrients (e.g., Fe, Mn) or can be used as proxies (e.g., REY) for mineral nutrients, thus lithologically controlled differences in redox conditions may also control mineral nutrient availability and, ultimately, the ecological functioning of the regolith.

In this work, we analyzed REY and other trace elements with depth in two deep, highly leached, ridgetop regolith profiles in a humid, tropical montane forest. Each profile has developed over a different bedrock lithology, granitic or andesitic volcaniclastic. Our objectives were to examine the effects of lithology on the critical zone processes (e.g., bedrock dissolution, dust deposition, redox fluctuations) that control trace element behavior at advanced stages of weathering and to identify the processes that decouple shallow and deep elemental cycles in thick regolith. Our general approach was to (1) analyze the sources of REY and trace elements to the critical zone on the timescale of regolith development, (2) determine the mass-transfer processes affecting trace element distributions and (3) integrate these results in the context of a range of published critical zone parameters from these regolith profiles, located in a well-studied Critical Zone Observatory.

We hypothesize that *within* each regolith profile, the shift in the predominant source of trace elements (atmospheric input at the surface, weathering at depth) and in the processes of elemental-cycling (e.g., vegetation cycling at the surface; transport and chemical reactions at depth) causes the decoupling of shallow elemental cycles from those in the deep regolith. We also hypothesize that, when comparing the two profiles, the differences in regolith mineralogy (Fe(III)-(hydr)oxides and

clay content) between the two parent lithologies will be expressed as measurable differences in the REY patterns, highlighting the relative importance of the different sources and mass-transfer processes to REY and trace element behavior.

2. FIELD SETTING

The Luquillo Critical Zone Observatory (LCZO) is an ideal platform for investigating trace element behavior under intense weathering conditions, as it contains a series of well-studied, highly weathered regolith profiles. The overarching theme of the LCZO is to investigate how two dominant lithologies, andesitic volcaniclastic and granitic (Fig. 1), determine the chemical and physical properties of the regolith, nutrient cycling and exports to the streams (Buss and White, 2012; Murphy and Stallard, 2012; Porder et al., 2015; Stallard, 2012; Yi-Balan et al., 2014). Previous work at the LCZO has shown that the regolith developed over both lithologies is highly leached, acidic and strongly depleted in base cations, but differs in key properties like particle size and abundance of primary and secondary minerals (e.g., Buss et al., 2017; Porder et al., 2015; Yi-Balan et al., 2014). The elemental differences between lithologies are also expressed in different nutrient availability to microbial communities throughout the regolith and to plants at the surface, as the volcaniclastic bedrock contains about 50% more Ca and P, 300% more Mg and 50% less K than the granitic rock (Mage and Porder, 2013; Porder et al., 2015).

Our volcaniclastic field site (B1S1) is located in the Bisley 1 catchment, a tributary of the Río Mameyes (Fig. 1). This catchment is underlain by the ~100 Ma Fajardo Formation, a marine-bedded, meta-volcaniclastic unit (Briggs and Aguilar-Cortes, 1980) composed mainly of plagioclase, chlorite, quartz, pyroxene, epidote, orthoclase, amphibole and prehnite (Table 1; Buss et al., 2013). Typically, the mineral grains are sand-sized or smaller. Primary minerals weather to kaolinite, other 1:1 lattice clays, and Fe- and Al-(hydro)oxides, leaving only quartz and minor chlorite as remnants of the primary mineral assemblage (Buss and White, 2012; Buss et al., 2017).

At the bedrock-regolith transition (>9.3 m depth), the volcaniclastic saprolite contains <3 wt% K-feldspar and <10 wt% Mg-rich chlorite (Buss et al., 2017). The saprolite is mantled by shallow soils (0.5-1.0 m thick) rich in clay and poor in quartz, classified as Typic Haplohumults (i.e., moderate to well-drained ultisols; Scatena 1989; Silver et al. 1994; Johnson et al., 2011) covered by mature Tabonuco (*Dacryodes excelsa)* forest (Scatena and Lugo, 1995). The average annual precipitation in Bisley is 3878 mm y^{-1} (Gioda et al., 2013), dominated by intense and brief storm events (Scatena, 1989), and the mean daily temperature fluctuates from 21.2 °C to 25.5 °C (Murphy and Stallard, 2012).

Our granitic field site (LG1) is located in the Río Icacos catchment, which feeds into the Río Blanco (Fig. 1). This catchment is underlain by the Río Blanco Quartz Diorite (currently classified as a tonalite; Buss et al., 2017), which intruded the surrounding volcaniclastic rocks about 49 to 42 Ma ago (Smith et al., 1998). The Río Blanco bedrock is medium- to coarse-grained and commonly contains plagioclase, quartz, amphibole and partially chloritized biotite (Table 1; Buss et al., 2008). This rock weathers to a saprolite composed of quartz, biotite, kaolinite and sesquioxides, capped by 0.5-1.0 m of soil (Murphy et al., 1998; Schulz and White, 1999; White et al., 1998). At the bedrock-regolith transition (>5.0 m), the granitic saprolite contains 13-14 wt% altered biotite and trace amounts of plagioclase (Lugolobi et al., 2010; Murphy et al., 1998; Pett-Ridge et al., 2009b). The overlying soil is classified as a Plinthic Haplohumult and is covered by mature Palo Colorado (*Cyrilla racemiflora*) forest. The site has a mean annual temperature between 22 and 23 ºC and a mean annual rainfall of 4050 mm, with little seasonal variation (Gioda et al., 2013; Table 1).

Within these two monolithologic catchments (Fig. 1), we focus on two ridgetop regolith profiles that have been previously studied (Buss et al., 2005, 2010, 2017; Chapela Lara et al., 2017; Liermann et al. 2015; Lugolobi et al., 2010; Minyard et al., 2011, 2012; Murphy et al., 1998; Pett-Ridge, 2009; Pett-Ridge et al., 2009a,b; Schulz and White, 1999; Siebert et al., 2015; White et al., 1998; Yi-Balan et al., 2014). Key observations from soil pits at both of our field sites include a thin

A horizon (<17 cm depth) and the presence of redoximorphic features (defined as color patterns caused by depletion or concentration of pigment compared to the matrix color, formed by oxidation/reduction of Fe or Mn coupled with their removal, translocation or accumulation, or a soil matrix color controlled by the presence of Fe(III); Schoeneberger et al., 2012). The redoximorphic features in the volcaniclastic regolith profile include black, red and orange masses and a bright red layer at ~1.3 m depth followed by a white layer made of *grus* at 1.5 m depth (Yi-Balan et al., 2014). In the granitic site, Yi-Balan et al. (2014) reported dark spots from 0.7 to 1.1 m depth and Buss et al. (2005) documented ~2–5-mm-thick layers of black Mn-oxide accumulations at various depths. These redoximorphic features are more marked and more frequent in the volcaniclastic regolith profile, where the mottling between ~1.3 and 1.5 m depth (Yi-Balan et al., 2014) indicates that Mn-oxides closely co-exist with lighter-colored, reduced Fe, while the bright red layer at the same depth indicates the presence of Fe(III) phases, especially hematite (α-Fe_2O_3; Schaetzl and Anderson, 2005).

In addition to the visible redoximorphic features, several properties of the volcaniclastic regolith change at around 1 m depth (Fig. 2). For example, bulk density increases ~20%, from 1.1 g cm^{-3} at 0.6 m depth to 1.3 g cm^{-3} between 0.9 and 1.2 m depth (Fig. 2a). Buss et al. (2017) also report that water content reaches a minimum (27 vol.%) from 0.9 m to 1.2 m, but Liermann et al. (2015) found that water content reached a maximum (76 vol.%) at this same depth on another sampling date (Fig. 2b), suggesting that the layer from 0.9 to 1.2 m depth may have more variable moisture conditions than the rest of the profile. The volcaniclastic regolith is generally strongly acidic (average pH = 3.6), but pH changes by nearly 2 units from 3.0 at 0.6 m depth to a maximum of 4.8 at 1.4 m depth (Fig. 2c).

In the granitic regolith, bulk density increases from 0.7 g cm^{-3} at the surface of the profile to 1.4 g cm^{-3} at 1.2 m depth, below which it remains more or less constant at about 1.3 g cm^{-3} (Fig. 2a). Water content ranges from 27 to 45 wt. % (Buss et al., 2005), with near-saturation occurring at

~1 and 6 m depth (Stonestrom et al., 1998). The pH of the granitic regolith is higher (average pH = 5.3) and less variable than in the volcaniclastic site, increasing gradually with depth (Fig. 2c). However, a distinction can be made between more acidic values above 3.3 m depth (average pH = 4.7) and only slightly acidic below 5.9 m depth (average pH = 6.2; Fig. 2c).

3. MATERIALS AND METHODS

3.1 Sample collection and elemental analyses

Two regolith cores were collected by hand-augering until refusal on the two ridgetop sites (9.3 m depth in the volcaniclastic, collected in 2007; and 7.5 m in the granitic site, collected in 2003), with the granitic core including ~2 m of the bedrock-regolith transition at the bottom (saprock 'rindlets' in Buss et al., 2005). The regolith pH was measured using a 1:1 mixture of soil and water. Regolith samples were homogenized, dried at 40^0C and sieved to <2 mm. Two volcaniclastic bedrock samples from drilled boreholes were selected for trace elemental analyses, as representative of the mineralogy and chemical composition of the bedrock (Buss et al., 2013). Three visually unweathered granitic samples were collected from a road cut near the regolith profile using a sledgehammer.

All samples were pulverized and homogenized then dissolved in a multi-acid digest (HF, HCl, HNO$_3$) and analyzed via ICP-MS at the United States Geological Survey (USGS, Menlo Park, CA) for the volcaniclastic bedrock and regolith, and at Cornell University for the granitic bedrock and regolith. During analyses, the ICP-MS was tuned to minimize oxide formation and oxide corrections were made using additional standards containing individual REE. For samples analyzed at the USGS, certified reference material rocks were used as standards (BCR-1, BHVO-1, BIR-1, G-2 and AGV-1). For samples analyzed at Cornell University, calibration standards were based on multi-element solutions and certified USGS reference material rocks were analyzed as unknowns.

Based on repeated analyses of samples and standards, the analytical uncertainty was estimated as 3%–5%.

3.2 Mass-transfer calculations

To determine losses or gains of labile elements throughout a regolith profile, the mass of an element of interest can be compared with the relative mass of an index element (i), assuming that the total stock of this index element does not change through time and that it has not been redistributed within the regolith (Brimhall et al., 1991a,b; Chadwick et al., 1990). The mass fraction of any element (j) added to or lost from the regolith during weathering, relative to the mass of the element originally present in the parent material, is calculated as the open-system mass transfer coefficient, commonly known as tau (Brimhall and Dietrich, 1987; Anderson et al., 2002):

$$\tau_{j,i} = \left(\frac{c_{j,w}}{c_{j,p}} \cdot \frac{c_{i,p}}{c_{i,w}} \right) - 1 \tag{1}$$

where $C_{j,w}$ is the concentration of an element j in the weathered material, $C_{j,p}$ is the concentration of the element in the parent material, and $C_{i,p}$ and $C_{i,w}$ refer to the concentrations of the index element in the bedrock and the weathered material, respectively. Negative values of $\tau_{j,w}$ indicate a net loss of element j from the regolith, while positive values indicate a net gain of the element relative to the bedrock.

Finally, to estimate the gain or loss of a given element in the regolith profile as a whole, relative to the contribution from bedrock weathering, we calculated an integrated mass-transfer value (τ_{int}) by weighting the mass transfer coefficient $\tau_{j,i}$ (Eq. 1) at each sampling depth by the product of the bulk regolith density (ρ) and the vertical distance (z) between measurements (Pett-Ridge et al., 2007):

$$\tau_{int} = \frac{\sum (\tau_h \, \rho_h \, z_h)}{\rho_t \, z_t} \tag{2}$$

where subscript *h* refers to values for individual sampling depths and the subscript *t* refers to total values for the entire profile.

3.3 REY normalization and anomalies

To enable comparison across the full group of REY despite their very different abundance in nature, REY concentrations of regolith samples (Tables 2 and 3) are normalized to the composition of the bedrock at each site. The Ce anomaly is calculated as the ratio of the observed Ce concentration and the value that would be expected for its atomic number (Ce*), obtained by linear interpolation between the two adjacent REE (La and Pr):

$$\frac{Ce}{Ce*} = \frac{2Ce_N}{(La_N + Pr_N)}$$

(3)

where Ce_N, La_N, Pr_N are the elemental concentrations normalized to the bedrock. By convention, Ce/Ce*>1 is referred to as a 'positive' Ce anomaly, which means Ce is preferentially retained in the regolith as compared to its neighboring REE and is indicative of oxidizing conditions. Conversely, a 'negative' Ce anomaly (Ce/Ce*<1) is indicative of anoxic conditions. Europium anomalies are calculated in a similar fashion:

$$\frac{Eu}{Eu^*} = \frac{2Eu_N}{(Sm_N + Gd_N)}$$

(4)

4. RESULTS

4.1 Mass transfer of trace elements

4.1.1 Conservative elements

We selected Nb as our index element because it is regarded as less mobile than Zr or Ti in tropical settings (Kurtz et al., 2001; Ma et al., 2007). The mass transfer coefficients $\tau_{j,Nb}$ (Eq. 1) of Ti, Zr, Hf

and Th are relatively constant from 1.8 m to the bottom of the volcaniclastic profile, as expected for conservative elements, but these elements are enriched towards the surface (Fig. 3a). In the granitic profile, Zr and Th are also enriched in the uppermost samples, and Th shows further signs of remobilization (Fig. 3b), which has been attributed to differential weathering of Th-bearing minerals in a study of a nearby regolith profile in this catchment (Chabaux et al., 2013).

4.1.2 Mobile elements

Both regolith profiles are strongly depleted in base cations as compared to the bedrock, with tau values from −1.0 for Ca to −0.8 for Mg (Table S2). However, in the volcaniclastic site, many metals show a modest but consistent relative increase above 1.2 m depth (Table 2; Fig. 3a,c,e). In the granitic site, alkali (e.g., Li, Na, K) and alkaline-earth metals (e.g., Mg, Ca, Sr) also show a depletion profile, becoming almost completely exhausted at the same depth at which the last of the bedrock plagioclase dissolves (5 m depth; Table S2).

Most of the elements known to change oxidation state in the weathering environment (Fe, Pb, Cr, V, Mn) are partially depleted throughout the volcaniclastic regolith as compared to the bedrock, with the greatest mass loss at 1.2 m depth (e.g., $\tau_{V,Nb}= − 0.84$), a modest mass gain towards the surface of the profile and a slight enrichment at 6.4 m depth (Fig. 3c). One notable exception to this behavior is Mn, which is enriched from 4.3 m to the bottom of the volcaniclastic profile, with a maximum enrichment of 145% at 6.4 m depth (Fig. 3c). In the granitic site, the behavior of redox-sensitive elements is mixed, with Fe and V depleted throughout the entire profile, while Mn, Cr and Pb are enriched by up to 475% at mid-depths (4.3-6.5 m; Fig. 3d).

4.1.3 Rare earth elements and yttrium (REY)

The volcaniclastic bedrock contains about 30% more REY than the granitic bedrock (ΣREY ≈ 77 µg g^{-1} and 59 µg g^{-1}, respectively; Tables 1 and 2) and similarly, REY concentrations are higher in the

volcaniclastic than in the granitic regolith (Tables 1 and 2). However, in terms of mass transfer coefficients (Eq. 1), REY contents are highly variable with depth, with both regolith profiles showing similar depletion-enrichment profiles, with the largest depletions at 1.2 m depth in the volcaniclastic (Fig. 3e) and at 0.9 m depth in the granitic profile (Fig. 3f). The largest REY enrichments are at mid-depths in both profiles (4.3 to 6.4 m), with slight enrichments above 1 m depth (Fig. 3e,f). The volcaniclastic regolith is more depleted in REY than the granitic regolith, especially in the uppermost 3 m of the profile (cf. Figs. 3e and 3f) and it is notable that REY contents fluctuate widely within a very short vertical distance from 1.2 to 0.6 m depth (Fig. 3e).

4.2 Bedrock-normalized REY patterns

4.2.1 LREE versus HREE trends

In the volcaniclastic site, normalized REE (Fig. 4a) show a concave upwards or 'bowl' pattern at medium depths (0.6 m and 1.2 to 2.7 m), due to a preferential loss of MREE, with regolith depleted in REE as compared to the bedrock ($REE_{regolith}/REE_{bedrock}<1$). A strong positive Ce anomaly and a small Eu anomaly develop at the same mid-depths (Fig. 4a). In contrast, surficial (0.0 to 0.3 m depth) and deeper regolith (8.2-4.3 m) show flat REE patterns, REE enrichments ($REE_{regolith}/REE_{bedrock}>1$) and slight negative Ce and Eu anomalies (Fig. 4a).

In the granitic site, the regolith is progressively depleted in most REE towards the surface, especially in the MREE and HREE (Fig. 4b), while the LREE are enriched as much as 4-fold relative to the granitic bedrock (Table 3). This enrichment in LREE towards the surface of the profile is also apparent in normalized La/Yb ratios (Fig. 5a). The volcaniclastic regolith is more enriched in Y at mid-depths than the granitic regolith, while the granitic regolith is more enriched in LREE than the volcaniclastic at both the surface and mid-depths (Fig. 3e,f).

The normalized REE patterns can also be used to evaluate fractionation *within* each REE group. Within the LREE group, represented by $(La/Pr)_N$, no fractionation is apparent from the

bottom of the profile up to 1.8 m depth in the volcaniclastic site and up to 5.7 m depth in the granitic site (Fig. 5b). Above these depths, La increases towards the surface in both profiles, more markedly in the granitic site (Fig. 5b). The $(Lu/Ho)_N$ ratios, an indicator of fractionation within the HREE group, are close to the bedrock composition below 4 m depth in both sites (Fig. 5c) and increase continuously above this depth in the granitic site and until 0.6 m depth in the volcaniclastic site. The most surficial samples in the volcaniclastic regolith return to bedrock-like $(Lu/Ho)_N$ values, also similar to Saharan dust values (Table 2).

4.2.2 REE anomalies

The Eu/Eu* values (Eq. 4) of the volcaniclastic regolith are similar to the bedrock in the deepest samples but a negative Eu anomaly develops at mid-depths, before returning to bedrock-like values near the surface of the profile (Fig. 5d). The granitic regolith shows a negative Eu anomaly below 5 m depth and at the surface of the profile, with bedrock-like values at mid-depths (Fig. 5d).

Cerium anomalies are larger and more variable in the volcaniclastic than in the granitic regolith (Fig. 6a,b). The volcaniclastic regolith profile exhibits well-developed positive Ce anomalies in most samples above 5 m depth, slight negative Ce anomalies below 6.4 m and no Ce anomaly (Ce/Ce* ≈ 1 in Eq. 3) at the surface of the profile (0.6-0 m depth; Fig. 6a). In contrast, the granitic regolith shows a small positive anomaly only at 4.3 m depth (Fig. 6b), coincident with an enrichment in Mn (Fig. 3d).

5. DISCUSSION

As weathering advances, chemical elements are removed from primary minerals and can be either leached or retained in the solid phase. As a result, the mass transfer ($\tau_{j,i}$, Eq. 1) of elements in a regolith profile can show four endmember trends with depth (Brantley and Lebedeva, 2011): *i)*

conservative, when an element remains relatively constant with depth due to its low mobility during weathering; *ii)* depletion, typical of highly soluble elements, which are lost as weathering advances towards the surface of a profile; *iii)* addition, when atmospheric inputs or biological cycling cause the enrichment of an element at the surface of a profile; or *iv)* depletion-enrichment, characteristic of elements that are leached at one depth but re-precipitate and accumulate deeper in the regolith.

In our regolith profiles, elements that are considered to be less mobile (Ti, Zr, Hf, Th) remain relatively constant with depth when normalized to the parent material (Eq. 1; Fig. 3a,b). In the other extreme, the highly soluble alkaline and alkaline-earth metals are almost completely lost from both regolith profiles (e.g., Mg, Ca, Sr; Tables 1, 2, S3). Finally, all REY (Fig. 3e,f) and many other redox-sensitive elements (Fig. 3c,d) show depletion-enrichment profiles, which are consistent with a processes of internal redistribution of trace elements, wherein (1) particles "move" upwards through the profile during weathering (as the ground surface and saprolite-bedrock interface are lowered); (2) reach the organically acidified environment of the soil, where they are mobilized into solution by crossing their pH sorption edge or by chelation to organic ligands; (3) percolate down deeper into the saprolite; and (4) are removed from solution into solid phases again when they reach a different Eh - pH environment or where organic ligands are less abundant.

Such internal redistribution of REY has been noted in other weathering profiles (e.g., Duddy, 1980; Ma et al., 2007; Nesbitt, 1979; Yusoff et al., 2013) and at corestone-rindlet sequences (Chabaux et al., 2013; Patino et al., 2003). Trace elements added via weathering of dust-derived minerals in near-surface regolith may also be redistributed by these dissolution-translocation-precipitation processes, as has been observed using Nd isotopes in the granitic profile (Pett-Ridge et al., 2009b).

5.1 Sources of trace elements and REY to the regolith profiles

Highly soluble elements (e.g., Ca, K, Mg, Sr) show depletion profiles in both the volcaniclastic and the granitic ridgetop sites (Table S2; Buss et al., 2017), i.e., tau decreases from the bottom to the surface of the profile, consistent with *in-situ* chemical weathering. Likewise, the negative Eu anomalies at 2.7-8.2 m depth (Fig. 5d) indicate that a Eu-bearing phase is dissolving preferentially as weathering proceeds, which is consistent with the dissolution of trace amounts of plagioclase in both lithologies (Buss and White, 2012; Buss et al., 2017; Porder et al., 2015; White et al., 1998). However, many trace elements are less-depleted above ~1 m depth in both profiles (Fig. 3a-f), some even showing an overall enrichment in the granitic profile (e.g., Th, Pb, Cr and La; Table S2). This enrichment, as well as the overall gain of REY (τ_{int} >1, Eq. 2; Table S2) indicate that, as well as bedrock weathering, an additional source is contributing to the elemental budget of the regolith profiles.

The fact that even relatively immobile elements (Fig. 3b) and elements that are not nutrients (Fig. 3c,d) are enriched in the regolith profiles (e.g., La τ_{int} = +1.5 in the granitic profile; Table S2), suggests that elements accumulate at the surface by atmospheric deposition and not by vegetation cycling. This atmospheric source is likely to be Saharan dust, which is estimated to account for up to 8 wt.% of shallow ridgetop soils over both lithologies at the LCZO (McClintock et al., 2015). The REE pattern of surficial samples in both of our regolith profiles is also consistent with Saharan dust input, which shows a continuous trend of decreasing REE enrichment with increasing atomic number (Fig. 4a,b). The negative Eu anomalies at the surface of both regolith profiles are also consistent with inputs of Saharan dust (Figs. 4a,b,5d).

5.2 Processes of mobilization and re-distribution of trace elements

The internal redistribution of cations that can be inferred from the depletion-enrichment profiles of REY (Fig. 3e,f) and other trace elements (Fig. 3c,d), may be related to pH changes. Most metals have sorption edges between pH 4 and 6, the same range we observe below 4 m depth in the granitic profile and at 1.5 and 4.8 m depth in the volcaniclastic profile (Fig. 2c). Indeed, the dissolution of plagioclase below 5 m depth in the granitic profile would buffer pH, in turn allowing for the precipitation or sorption of several elements from the porewater when it percolates down to that depth. Similarly, the pH shift of about 2 units at ~5 m depth in the volcaniclastic profile might cause the REY and Mn enrichment at 6.4 m depth (Fig. 3c). However, the similar pH increase at 1.5 m depth (Fig. 2c) in the volcaniclastic regolith is not associated with trace element accumulations (Fig. 3a,c,e). On the contrary, REY and most other trace elements are strongly depleted at and below 1.5 m, suggesting another process, likely related to organic matter complexation or secondary mineralogy, is controlling REY mobility in the upper half of the volcaniclastic profile.

In addition to pH effects, depletion-enrichment profiles of metals have also been attributed to chelation by organic ligands in the surface layers of regolith, followed by eluviation and precipitation at lower depths where organic ligands are less abundant (e.g., Atkinson and Wright, 1957; Jin et al., 2017). However, soil organic carbon is very low (<1.5%) in both profiles below about 30 cm, dropping to <0.3% below about 100 cm (Stone et al., 2014; Buss et al., 2005; Yi-Balan et al., 2014) and therefore eluviation of ligand-bound metals is unlikely to reach the depths of the enrichments (~ 4-8 m depth for Mn and some REY, Fig. 3c,e) before the ligands are scavenged.

The depletion-enrichment profiles of REY could also be driven by changes in the secondary mineralogy as weathering advances, because aqueous metal concentrations are often determined by partitioning into secondary minerals. A common mineralogical evolution in tropical weathering is the aging of short-range-order phases such as gibbsite and ferrihydrite to purer, more crystalline phases such as goethite, hematite and kaolinite (Chadwick and Chorover, 2001; Chorover et al.,

2004; Ziegler et al., 2005). The less-evolved, short-order phases are associated with higher concentrations of trace elements (Nalovic and Janot, 1979; Nalovic and Pint, 1972). For instance, Martinez and McBride (1998) demonstrated that large ionic radius ions such as Pb^{2+} are expelled during ageing of Fe-oxides, which also tend to expel REEs during ageing and crystallization (Laveuf and Cornu, 2009). Therefore, the re-crystallization of Fe or Mn-oxides as weathering advances would be accompanied by expulsion of adsorbed or co-precipitated trace elements with a preference for the larger radii ions, like the LREE. This mechanism can account for the general decrease in REY concentrations from 6 m depth to the surface of the profiles, but not for the larger enrichment of all REE at mid-depths (Fig. 3e,f). The coincident enrichments of REY and Mn at mid-depths in both regolith profiles (Fig. 3c-f) is instead consistent with the strong influence of the redox chemistry of Mn on the behavior of REY (Devranche et al., 2005), which is discussed in the following sections.

5.3 Processes of REY fractionation

Heavy REE are more easily leached during weathering than LREE (e.g., Goldstein and Jacobsen, 1988; Ma et al., 2002; Laveuf and Cornu, 2009, and references therein). Therefore, when observing REE variations with depth in regolith profiles, we would expect to see: (*i*) an increasing LREE/HREE ratio from the bottom to the top of a profile, reflecting the longer duration of weathering further from the bedrock; and (*ii*) a greater LREE/HREE ratio in the most weathered profiles when comparing profiles with differing degrees of weathering.

The granitic regolith exemplifies the expected LREE/HREE fractionation with depth, showing a progressive enrichment in the less soluble LREE towards the surface of the profile (Figs. 4b, 5a). In contrast, the volcaniclastic regolith shows little LREE/HREE fractionation, despite being relatively more weathered than the granitic profile (Fig. S1, Table S1), opposite to what we expected from comparison to previous studies (e.g., Nesbitt et al., 1990; Ma et al., 2007; Yusoff et

al., 2013). These differing LREE/HREE patterns may stem from the differences in secondary mineralogy between the two profiles, which in turn influence REY retention or leaching via sorption/desorption and precipitation/dissolution processes (Fig. 7a,b). For example, the volcaniclastic regolith contains more kaolinite and goethite (Table 1), which preferentially retain LREE (Laveuf and Cornu, 2009). Also, LREE are preferentially retained in secondary minerals after primary mineral dissolution (Nesbitt, 1979) but can later be released when secondary minerals dissolve or age in extreme weathering environments.

The concave-upward or 'bowl-shaped' REE pattern near the surface of the granitic regolith (Fig. 4b) and at mid-depths in the volcaniclastic regolith (Fig. 4a), indicates a preferential loss of MREE, which could be caused by preferential leaching of MREE bound to organic matter (Laveuf and Cornu, 2009). However, as previously mentioned, organic carbon is very low in both regolith profiles (Buss et al., 2005; Stone et al., 2014; Yi-Balan et al., 2014). Therefore, the fractionation of HREE (Yb) and LREE (La) with respect to MREE (Gd) in the LCZO profiles likely results from inorganic leaching and sorption processes (Fig. 7a,b).

In this framework, the most remarkable difference in REE fractionation patterns between the two sites is at shallow to intermediate depths (0.6-1.8 m in the volcaniclastic regolith and 1.5-4.3 m in the granitic regolith). At these depths, the volcaniclastic regolith is somewhat enriched in LREE and more significantly in the HREE, relative to the bedrock (Fig. 7a), whereas in the granitic regolith LREE are more enriched than in the volcaniclastic and HREE enrichment is insignificant (Fig. 7b). This difference likely stems from the high sensitivity of REE to adsorption/desorption reactions (Devranche et al., 2005), with HREE more strongly sorbed than LREE due to their smaller ionic radii (the lanthanide contraction effect; Laveuf and Cornu, 2009). Therefore, the differentiated REE fractionation between the two sites might be expressing the predominance of dissolution/precipitation versus sorption/desorption as the process controlling the redistribution of REE within the two regolith profiles (Fig. 7a,b). This difference in the predominant process can be

attributed to the greater total abundance of sorbing phases, such as clays and metal (hydr)oxides, in the volcaniclastic as compared to the granitic regolith (Buss et al., 2017; McClintock et al., 2015). A change from leaching to sorption as the dominant REE translocation process could also explain the LREE/HREE pattern throughout the volcaniclastic regolith, with leaching dominant below 4.3 m and sorption comparatively more important above 0.6 m depth (i.e., in the rooting zone), where organic matter and short-range order (high surface area) minerals are relatively more abundant.

5.4 Redox controls on REY in the regolith

As discussed in Sections 5.1 and 5.2, the redistribution of trace elements in the granitic profile can be explained by dust and weathering inputs and associated pH changes. However, trace element distributions in the volcaniclastic profile do not correspond to pH changes (Fig. 8a,d). Instead, the depletion-enrichment profiles of REY (Fig. 3e,8d) and other redox-sensitive elements (Fig. 3c) in the volcaniclastic profile are consistent with variations in redox conditions, which in turn would promote the dissolution of phases holding trace elements in the upper layers of the profile (e.g., Fe(III)-hydroxides), followed by transport and precipitation in the deeper layers where Eh-pH conditions are different.

The gaseous and the solid-phase composition of these two deep regolith profiles provide information about their current redox conditions, but also a measure of the integrated longer-term redox status of the regolith, as expressed in the Ce anomaly and in the distributions of REY and other redox-sensitive elements (Fig. 6a,b). Currently, the regolith profiles over both lithologies are generally well-aerated down to the depth of auger refusal (7.5 m in the granitic and 9.3 m in the volcaniclastic regolith) as determined by visual inspection, hydraulic saturation values (Buss et al., 2017; Stonestrom et al., 1998) and O_2 contents in the regolith atmosphere (Buss et al., 2017; Hall et al., 2016). However, the O_2 content is more variable with depth in the volcaniclastic than in the granitic profile (Fig. 6). Oxygen sensors installed in the granitic regolith logged hourly over two

years revealed fluctuations of <10 vol.% near the surface, but little fluctuation below 0.5 m (<1.5 vol.% O_2; Hall et al., 2016), while static measurements in the volcaniclastic regolith (0.6, 1.8, 2.7, 3.7, 4.9 and 7.3 m depths) indicated a drop in O_2 of roughly 5% below 2 m depth (Fig. 6a; Buss et al., 2017).

Redox conditions integrated over the timescale of regolith development, reflected by the Ce anomaly, are also noticeably different between the two sites, with higher and more variable Ce/Ce* values in the volcaniclastic than in the granitic profile (Fig. 6a,b). The larger variation in Ce/Ce* values in the volcaniclastic profile likely reflects stronger redox fluctuations, a consequence of more variation in water saturation and O_2 contents. These redox fluctuations would promote the local redistribution of Ce when Fe and Mn oxides are subjected to reductive dissolution, as Ce(IV) is then released to the soil solution and scavenged by Fe and Mn oxides in nearby oxidizing areas. In contrast, the granitic regolith has higher sand and lower clay contents (Buss et al., 2005), making it more uniformly oxic throughout (Fig. 6b) and not promoting the retention/re-mobilization of Ce at most depths. As a result, the granitic regolith shows a positive Ce anomaly only at 4.3 m depth (Fig. 6b), consistent with pH-controlled adsorption or coprecipitation of Ce(IV) to Mn-oxides at the depth of maximum Mn enrichment (Fig. 3d).

We propose that the maximum Ce/Ce* value at ~1.8 m in the volcaniclastic profile constitutes a long-term redox front at the same depth of the maximum contemporary O_2 content (Fig. 6a). This oxidizing front divides the volcaniclastic regolith into two redox domains: an upper, oxic, environment and a deeper, less oxic environment (Figs. 6a, 8). However, within the oxidizing domain, there are important redox fluctuations in the short- and long-term, especially between 0.9 and 1.5 m depth. These fluctuations are indicated by the visible redoximorphic features and the Ce anomaly, which varies substantially within a short vertical distance, suggesting locally reducing or oscillating redox conditions during the timescale of regolith formation (Fig. 6a). Expulsion of co-precipitated or adsorbed trace elements during oscillating redox conditions (e.g., Liptzin et al.,

2011; Thompson et al. 2006) could give rise to the anomalous features observed at about 1 m depth, including the HREE and LREE fractionation patterns (Fig. 7a), the large depletion in most trace elements (Figs. 3a,c,e) and the absence of a positive Ce anomaly (Fig. 6a).

The differences in redox conditions between the two sites likely stem from differences in moisture dynamics due to differing regolith texture, causing differing permeability, with periodic saturation leading to depletion of O_2 after rainfall events. As the differences in the regolith texture and permeability largely result from the differences in the bedrock initial grain size, porosity and mineralogy (Buss et al., 2017), the observed hydrologic control on redox conditions and trace element behavior would be ultimately controlled by lithology.

5.5 Decoupling of shallow and deep critical zone processes

The processes that add, transport, or transform REY and trace elements in the critical zone also affect other inorganic elements, including mineral nutrients and micronutrients. Furthermore, differences in the source of elements (e.g., dust or weathering) and in redox conditions with depth can not only affect element distributions and cycles, but also biological communities. The enrichment in most trace elements (Fig. 3a-f) and the negative Eu anomalies (Fig. 4,5d) near the surface of both profiles suggest an atmospheric input (Section 5.1). Likewise, the LREE enrichment in the surface layers of the regolith profiles (Fig. 4,7), although also somewhat affected by pedogenic processes, is consistent with input of Saharan dust, in agreement with previous studies that found dust to be an important source of trace metals and limiting nutrients to LCZO soils (Chapela Lara et al., 2017; McClintock et al., 2015; Pett-Ridge, 2009; Pett-Ridge et al., 2009b). In fact, atmospheric inputs allow LCZO soils to maintain relatively high cation stocks despite the near-total depletion of the bedrock source (Porder et al., 2015). In contrast, at the bottom of the regolith profiles, nutrients and micronutrients are sourced from weathering bedrock (Buss et al., 2005; 2010; Chapela Lara et al., 2017; Yi-Balan et al., 2014). The mid-depths of deep, highly weathered,

tropical regolith are left with limited or no access to either the dust or bedrock sources of mineral nutrients, contributing to the decoupling of nutrient cycles and microbial communities (e.g., Buss et al., 2005).

In addition to the vertical separation of the sources of mineral nutrients to the shallow and deep regolith, the fluctuating redox conditions from 0.9 to 1.5 m depth (Section 5.4) may also contribute to the decoupling of the shallow and deep microbial communities in the volcaniclastic regolith (Fig. 8b,c). In effect, this redox hot-spot defines a transition between the upper, oxic, chemoheterotrophy-dominated microbial communities, supported by the photoautotrophic primary production of the forest, and the deeper, suboxic microbial communities driven by chemolithoautotrophic primary production. When redox conditions change from oxic to anoxic, resident microbial communities change as well, such that species that can utilize an anaerobic metabolism proliferate and those that cannot die or become dormant. If the environment then becomes oxic, obligately anaerobic species will be replaced by facultative or aerobic microorganisms. Redox oscillations may therefore limit the growth of all microorganisms, regardless of their metabolic strategy. Indeed, this interpretation is consistent with microbial cell numbers around the volcaniclastic redox hot-spot, including a localized drop of about two orders of magnitude in total microbial cells at 1.1 m depth relative to the cell numbers above and below (Fig. 8c), a drop of one order of magnitude in Fe-related bacteria at that same depth and the presence of anaerobic bacteria at 1.4, 1.8 and 2.5 m depth (Liermann et al., 2015).

Other salient layers in terms of geomicrobiological interactions occur at 4.3-6.4 m depth in the volcaniclastic regolith (Fig. 3c,e) and at 4.3-5.3 m depth in the granitic regolith (Fig. 3d,f), where Mn, REY and other redox-sensitive elements are enriched, indicating that Mn oxides are precipitating at those depths. Natural Mn oxides in soils are largely considered to be biogenic, produced by oxidation of Mn(II) by chemolithoautotrophic microorganisms (e.g., Tebo et al., 2005). These layers of Mn+trace element enrichment may therefore constitute hot-spots for microbial

communities in these organic carbon-poor environments, as exemplified by increases in groups of microorganisms exploiting various metabolic strategies at these depths in the volcaniclastic profile (Liermann et al., 2015). The spatial coincidence of these elemental and microbial enrichments (Fig. 8b-d) suggests that the volcaniclastic regolith fosters an ecosystem of chemoheterotrophs (some reducing Fe(III) or Mn(IV) in anoxic microenvironments, with others reducing O_2 in oxic environments) consuming organic carbon produced by chemolithoautotrophs that oxidize Fe(II) or Mn(II) and fix CO_2, similar to earlier findings in the granitic regolith (Buss et al., 2005; Hall et al., 2016).

6. CONCLUSIONS

We analyzed the variation of REY and other trace elements with depth and lithology in two highly-leached, ridgetop regolith profiles, to better understand their behavior during weathering in the humid tropics and to elucidate the mechanisms by which deep elemental cycles become decoupled from those near the surface. We observed some similarities between the two sites: both regoliths show depletion profiles, formed by the loss of most cations as weathering advances, and both exhibit evidence of atmospheric input at the surface of the profiles, as expected. However, we also found significant differences in trace element distributions, REY fractionation and translocation, and redox dynamics.

In the granitic regolith, the dissolution of residual plagioclase buffers the pH to less-acidic values below 5 m depth, allowing for several trace elements to re-precipitate at that depth. In contrast, in the volcaniclastic regolith, pH control is apparently less important than changes in Eh, which affect the fractionation and translocation of REY and other redox-sensitive elements through sorption/desorption reactions. The most significant distinction between the two profiles is the long-term redox conditions as a function of depth, more variable and stratified in the volcaniclastic profile and changing gradually in the granitic profile; this difference is controlled by textural

differences, which stem from the different parent lithology (volcaniclastic andesitic vs. granitic) of the two neighboring sites.

Based on the Ce anomaly variation with depth, the volcaniclastic regolith can be divided into two domains: an upper, biologically controlled, oxic domain; and a deeper, less oxic and geochemically controlled domain. The crucial threshold that separates the surface from the deep environment is a layer where redox conditions fluctuate over time, as interpreted from a wide range of geochemical and physical parameters. Within this layer, trace elements are more easily leached, driven by dissolution/precipitation. The low trace element concentrations and the oscillating redox conditions may also represent a threshold for microbial communities.

The behavior of trace elements in our regolith profiles provides further evidence of the importance of atmospheric inputs as a source of nutrients for shallow ecosystems in highly weathered regolith, which can be decoupled from the deep ecosystems that depend on bedrock weathering inputs at depth. However, our work highlights how *internal* controls (such as pH and redox changes) determine the translocation of trace elements throughout deep regolith profiles, such that the fate of trace elements is modulated by a complex set of overlapping leaching, sorption, and precipitation processes. Ultimately, these internal controls stem from the underlying lithology even at advanced stages of weathering.

REFERENCES

Anderson, S.P., Dietrich, W.E., Brimhall, G.H., 2002. Weathering profiles, mass-balance analysis, and rates of solute loss: Linkages between weathering and erosion in a small, steep catchment. Geological Society of America Bulletin, 114: 1143-1158.

Atkinson, H.J., Wright, J.R., 1957. Chelation and the Vertical Movement of Soil Constituents. Soil Science, 84(1): 1-12.

Banfield, J.F., Eggleton, R.A., 1989. Apatite replacement and rare earth mobilization, fractionation, and fixation during weathering. Clays and Clay Mineralogy, 37: 113-127.

Bau, M., 1999. Scavenging of dissolved yttrium and rare earths by precipitating iron oxyhydroxide: Experimental evidence for Ce oxidation, Y-Ho fractionation, and lanthanide tetrad effect. Geochim. Cosmochim. Acta, 63: 67-77.

Bau, M., Koschinsky, A., 2009. Oxidative scavenging of cerium on hydrous Fe oxide: Evidence from the distribution of rare earth elements and yttrium between Fe oxides and Mn oxides in hydrogenetic ferromanganese crusts. Geochemical Journal, 43: 37-47.

Brantley, S.L., Bandstra, J., Moore, J., White, A.F., 2008. Modelling chemical depletion profiles in regolith. Geoderma, 145(3–4): 494-504.

Brantley, S.L., Lebedeva, M., 2011. Learning to Read the Chemistry of Regolith to Understand the Critical Zone. Annual Review of Earth and Planetary Sciences, 39(1): 387-416.

Brantley, S.L., White, A.F., 2009. Approaches to Modeling Weathered Regolith. Reviews in Mineralogy and Geochemistry, 70: 435-484.

Braun, J.-J. et al., 2012. Elemental weathering fluxes and saprolite production rate in a Central African lateritic terrain (Nsimi, South Cameroon). Geochimica et Cosmochimica Acta, 99: 243-270.

Braun, J.J. et al., 2005. Present weathering rates in a humid tropical watershed: Nsimi, South Cameroon. Geochimica et Cosmochimica Acta, 69(2): 357-387.

Braun, J.J., Pagel, M., Herbillon, A., Rosin, C., 1993. Mobilization and redistribution of REEs and thorium in a syenitic lateritic profile: a mass balance study. Geochimica et Cosmochimica Acta, 57(18): 4419-4434.

Braun, J.J. et al., 1998. Solid/liquid REE fractionation in the lateritic system of Goyoum, East Cameroon: the implication for the present dynamics of the soil covers of the humid tropical regions. Geochimica et Cosmochimica Acta, 62(2): 273-300.

Briggs, R.P., Cortes-Aguilar, E., 1980. Geologic map of the Fajardo and Cayo Icacos quadrangles, Puerto Rico. U.S. Geological Survey.

Brimhall, G.H., Chadwick, O.A., Lewis, C.J., Compston, W., Williams, I.S., Danti, K.J., Dietrich, W.E., Power, M.E., Hendricks, D., Bratt, J., 1991a. Deformational mass transport and invasive processes in soil evolution. Science, 255(5045): 695-702.

Brimhall, G.H. et al., 1991b. Quantitative geochemical approach to pedogenesis: importance of parent material reduction, volumetric expansion, and eolian influx in lateritization. Geoderma, 51(1–4): 51-91.

Brimhall, G.H., Dietrich, W.E., 1987. Constitutive mass balance relations between chemical composition, volume, density, porosity, and strain in metasomatic hydrochemical systems: results on weathering and pedogenesis. Geochimica et Cosmochimica Acta, 51(3): 567-587.

Bruijnzeel, L.A., 1991. Nutrient input-output budgets of tropical forest ecosystems: A review. Journal of Tropical Ecology, 7(1): 1-24.

Buss, H.L. et al., 2013. Probing the deep critical zone beneath the Luquillo Experimental Forest, Puerto Rico. Earth Surface Processes and Landforms, 38(10):1170-1186.

Buss, H.L. et al., 2005. The coupling of biological iron cycling and mineral weathering during saprolite formation, Luquillo Mountains, Puerto Rico. Geobiology, 3(4): 247-260.

Buss, H.L. et al., 2017. Lithological influences on contemporary and long-term regolith weathering at the Luquillo Critical Zone Observatory. Geochimica et Cosmochimica Acta, 196: 224-251.

Buss, H.L., Sak, P.B., Webb, S.M., Brantley, S.L., 2008. Weathering of the Rio Blanco quartz diorite, Luquillo Mountains, Puerto Rico: Coupling oxidation, dissolution, and fracturing. Geochimica et Cosmochimica Acta, 72: 4488-4507.

Buss, H.L., White, A., 2012. Weathering Processes in the Icacos and Mameyes Watersheds in Eastern Puerto Rico. In: Murphy, S.F.S., R. (Ed.), Water Quality and Landscape Processes of Four Watersheds in Eastern Puerto Rico. Profesional Paper. US Geological Survey, Reston, Virginia, pp. 249-287.

Butt, C.R.M., Lintern, M.J., Anand, R.R., 2000. Evolution of regoliths and landscapes in deeply weathered terrain — implications for geochemical exploration. Ore Geology Reviews, 16(3): 167-183.

Byrne, R.H., Li, B., 1995. Comparative complexation behavior of the rare earths. Geochimica et Cosmochimica Acta, 59: 4575 - 4589.

Chabaux, F. et al., 2013. Regolith formation rate from U-series nuclides: Implications from the study of a spheroidal weathering profile in the Rio Icacos watershed (Puerto Rico). Geochimica et Cosmochimica Acta, 100: 73-95.

Chadwick, O.A., Brimhall, G.H., Hendricks, D.M., 1990. From black box to a grey box: a mass balance interpretation of pedogenesis. Geomorphology, 3: 369-390.

Chadwick, O.A., Chorover, J., 2001. The chemistry of pedogenic thresholds. Geoderma, 100: 321-353.

Chadwick, O.A., Derry, L.A., Vitousek, P.M., Huebert, B.J., Hedin, L.O., 1999. Changing sources of nutrients during four million years of ecosystem development. Nature, 397(6719): 491-497.

Chapela Lara, M., Buss, H.L., Pogge von Strandmann, P.A.E., Schuessler, J.A., Moore, O.W., 2017. The influence of critical zone processes on the Mg isotope budget in a tropical, highly weathered andesitic catchment. Geochimica et Cosmochimica Acta, 202: 77-100.

Chorover, J., Amistadi, M.K., Chadwick, O.A., 2004. Surface charge evolution of mineral-organic complexes during pedogenesis in Hawaiian basalt. Geochimica et Cosmochimica Acta, 68(23): 4859-4876.

Clergue, C. et al., 2015. Influence of atmospheric deposits and secondary minerals on Li isotopes budget in a highly weathered catchment, Guadeloupe (Lesser Antilles). Chemical Geology, 414(): 28-41.

De Carlo, E.H., Wen, X.Y., Irving, M., 1998. The influence of redox reactions on the uptake of dissolved Ce by suspended Fe and Mn oxide particles. Aquatic Geochemistry, 3: 357-389.

De Kimpe, C.R., Laverdiere, M.R., Dejou, J., Lasalle, P., 1984. Effects of acidic and basic parent materials on formation of some soils in Quebec (Canada). Geoderma, 33(2): 101-118.

Derry, L.A., Chadwick, O.A., 2007. Contributions from Earth's Atmosphere to Soil. Elements, 3(5): 333.

Devranche, M., Pourret, O., Gruau, G., Dia, A., Le Coz-Bouhnik, M., 2005. Adsorption of REE(III)-humate complexes onto MnO2: Experimental evidence for cerium anomaly and lanthanide tetrad effect suppression. Geochimica et Cosmochimica Acta, 69(20): 4825–4835.

Dosseto, A., Buss, H.L., Suresh, P.O., 2012. Rapid regolith formation over volcanic bedrock and implications for landscape evolution. Earth and Planetary Science Letters, 337-338: 47-55.

Duddy, L.R., 1980. Redistribution and fractionation of rare-earth and other elements in a weathering profile. Chemical Geology, 30(4): 363-381.

Ebelmen, J.J., 1845. Sur les produits de la d´ecomposition des esp`eces min´erales de la famille des silicates. Annales des Mines 7, 3–66.

Elderfield, H., Upstill-Goddard, R., Sholkovitz, E.R., 1990. The rare earth elements in rivers, estuaries, and coastal seas and their significants to the composition of ocean waters. Geochimica et Cosmochimica Acta, 54: 971-991.

Fletcher, R.C., Brantley, S.L., 2010. Reduction of bedrock blocks as corestones in the weathering profile: observations and model. American Journal of Science, 310: 131-164.

Fritz, S.J., 1988. A comparative study of gabbro and granite weathering. Chemical Geology, 68(3): 275-290.

Gioda, A. et al., 2013. Chemical constituents in clouds and rainwater in the Puerto Rican rainforest: Potential sources and seasonal drivers. Atmospheric Environment, 68: 208-220.

Goldstein, S.J., Jacobsen, S.B., 1988. Rare earth elements in river waters. Earth and Planetary Science Letters, 89: 35-47.

Hall, S.J., Liptzin, D., Buss, H.L., DeAngelis, K., Silver, W.L., 2016. Drivers and patterns of iron redox cycling from surface to bedrock in a deep tropical forest soil: a new conceptual model. Biogeochemistry, 130(1): 177-190.

Harden, J.W., 1982. A quantitative index of soil development from field descriptions: examples from a chronosequence in central California. Geoderma, 28(1): 1-28.

Harlavan, Y., Erel, Y., 2002. The release of Pb and REE from granitoids by the dissolution of accessory phases. Geochimica et Cosmochimica Acta, 66(5): 837-848.

Henderson, P., 1984. General geochemical properties and abundances of the rare earth elements. In: Henderson, P. (Ed.), Rare Earth Element Geochemistry. Developments in Geochemistry. Elsevier, Amsterdam.

Hewawasam, T. et al., 2013. Slow advance of the weathering front during deep, supply-limited saprolite formation in the tropical Highlands of Sri Lanka. Geochimica et Cosmochimica Acta, 118: 202-230.

Huffaker, L., 2002. Soil Survey of Caribbean National Forest and Luquillo Experimental Forest, Commonwealth of Puerto Rico. USDA-NRCS, 181 pp.

Jiang, K., Qi, H.-W., Hu, R.-Z., 2018. Element mobilization and redistribution under extreme tropical weathering of basalts from the Hainan Island, South China. Journal of Asian Earth Sciences, 158: 80-102.

Jin, L. et al., 2017. REE mobility and fractionation during shale weathering along a climate gradient. Chemical Geology, 466(Supplement C): 352-379.

Johnson, K.D., Scatena, F.N., Silver, W.L., 2011. Atypical soil carbon distribution across a tropical steepland forest catena. Catena, 87: 391-397.

Kurtz, A.C., Derry, L.A., Chadwick, O.A., 2001. Accretion of Asian dust to Hawaiian soils: isotopic, elemental, and mineral mass balances. Geochimica et Cosmochimica Acta, 65(12): 1971-1983.

Kurtz, A.C., Derry, L.A., Chadwick, O.A., Alfano, M.J., 2000. Refractory element mobility in volcanic soils. Geology, 28(8): 683-686.

Larsen, M.C., 2012. Landslides and sediment budgets in four watersheds in eastern Puerto Rico, in: Murphy, S.F.S., R.F. (Ed.), Water quality and landscape processes of four watersheds in eastern Puerto Rico: U.S. Professional Paper 1789, p. 153–178. USGS, pp. 153-178.

Laveuf, C., Cornu, S., 2009. A review on the potentiality of Rare Earth Elements to trace pedogenetic processes. Geoderma, 154: 1-12.

Liermann, L.J., Albert, I., Buss, H.L., Minyard, M., Brantley, S.L., 2015. Relating Microbial Community Structure and Geochemistry in Deep Regolith Developed on Volcaniclastic Rock in the Luquillo Mountains, Puerto Rico. Geomicrobiology Journal, 32(6): 494-510.

Liptzin, D., Silver, W.L., Detto, M., 2011. Temporal dynamics in soil oxygen and greenhouse gases in two humid tropical forests. Ecosystems, 14: 171-182.

Lugolobi, F., Kurtz, A.C., Derry, L.A., 2010. Germanium-silicon fractionation in a tropical, granitic weathering environment. Geochimica et Cosmochimica Acta, 74: 1294-1308.

Ma, J.-L., Wei, G.-J., Xu, Y.-G., Long, W.-G., Sun, W.-D., 2007. Mobilization and re-distribution of major and trace elements during extreme weathering of basalt in Hainan Island, South China. Geochimica et Cosmochimica Acta, 71(13): 3223-3237.

Mage, S.M., Porder, S., 2013. Parent Material and Topography Determine Soil Phosphorus Status in the Luquillo Mountains of Puerto Rico. Ecosystems, 16(2): 284-294.

Martinez, C.E., and McBride, M.B., 1998, Coprecipitates of Cd, Cu, Pb and Zn in iron oxides: Solid phase transformation and metal solubility after aging and thermal treatment. Clays and Clay Minerals, 46: 537-545.

McClintock, M.A., Brocard, G., Willenbring, J., Tamayo, C., Porder, S., Pett-Ridge, J.C., 2015. Spatial variability of African dust in soils in a montane tropical landscape in Puerto Rico. Chemical Geology, 412: 69-81.

Merrill, G.P., 1906. A Treatise on Rocks, Rock Weathering and Soils. MacMillian Inc., New York.

Minyard, M.L., Bruns, M.A., Liermann, L.J., Buss, H.L., Brantley, S.L., 2012. Bacterial Associations with Weathering Minerals at the Regolith-Bedrock Interface, Luquillo Experimental Forest, Puerto Rico. Geomicrobiology Journal, 29(9): 792-803.

Minyard, M.L. et al., 2011. Halloysite nanotubes and bacteria at the saprolite-bedrock interface, Rio Icacos Watershed, Puerto Rico. Soil Science Society of America Journal, 75(2): 348-356.

Muhs, D.R., Budahn, J.R., Prospero, J.M., Carey, S.N., 2007. Geochemical evidence for African dust inputs to soils of western Atlantic islands: Barbados, the Bahamas, and Florida. Journal of Geophysical Research, 112: F02009.

Murphy, S.F., Brantley, S.L., Blum, A.E., White, A.F., Dong, H., 1998. Chemical weathering in a tropical watershed, Luquillo Mountains, Puerto Rico; II. Rate and mechanism of biotite weathering. Geochimica et Cosmochimica Acta, 62(2): 227-243.

Murphy, S.F., Stallard, R.F., 2012. Hydrology and climate of four watersheds in eastern Puerto Rico. In: Murphy, S.F., Stallard, R.F. (Eds.), Water quality and landscape processes of four watersheds in eastern Puerto Rico, pp. 47-83.

Nahon, D., Merino, E., 1997. Pseudomorphic replacement in tropical weathering; evidence, geochemical consequences, and kinetic-rheological origin. American Journal of Science, 297(4): 393-417.

Nalovic, L., Janot, C., 1979. Mössbauer study of the crystallogenesis of iron hydroxides. Rev. Phys. Appl. (Paris), 14(3): 475-480.

Nalovic, L., Pint, M., 1972. Recherches sur les elements traces dans les sols tropicaux: Etude de quelques sols du Cameroun. Geoderma, 7(3): 249-267.

Navarre-Sitchler, A., Brantley, S.L., Rother, G., 2015. How Porosity Increases During Incipient Weathering of Crystalline Silicate Rocks. Reviews in Mineralogy and Geochemistry, 80(1): 331-354.

Nesbitt, H.W., 1979. Mobility and fractionation of rare earth elements during weathering of a granodiorite. Nature, 279(5710): 206-210.

Nesbitt, H.W., MacRae, N.D., Kronberg, B.I., 1990. Amazon deep-sea fan muds: light REE enriched products of extreme chemical weathering. Earth and Planetary Science Letters, 100(1–3): 118-123.

Nesbitt, H.W., Markovics, G., 1997. Weathering of granodioritic crust, long-term storage of elements in weathering profiles, and petrogenesis of siliciclastic sediments. Geochim. Cosmochim. Acta, 61: 1653-1670.

Nesbitt, H.W., Young, G.M., 1982. Early Proterozoic climates and plate motions inferred from major element chemistry of lutites. Nature, 199: 715-717.

Patino, L.C., Velbel, M.A., Price, J.R., Wade, J.A., 2003. Trace element mobility during spheroidal weathering of basalts and andesites in Hawaii and Guatemala. Chemical Geology, 202(3): 343-364.

Pett-Ridge, J., 2009. Contributions of dust to phosphorus cycling in tropical forests of the Luquillo Mountains, Puerto Rico. Biogeochemistry, 94(1): 63-80.

Pett-Ridge, J.C., Derry, L.A., Barrows, J.K., 2009a. Ca/Sr and 87Sr/86Sr ratios as tracers of Ca and Sr cycling in the Rio Icacos watershed, Luquillo Mountains, Puerto Rico. Chemical Geology, 267(1): 32-45.

Pett-Ridge, J.C., Derry, L.A., Kurtz, A.C., 2009b. Sr isotopes as a tracer of weathering processes and dust inputs in a tropical granitoid watershed, Luquillo Mountains, Puerto Rico. Geochimica et Cosmochimica Acta, 73: 25-43.

Pett-Ridge, J.C., Monastra, V.M., Derry, L.A., Chadwick. O.A., 2007. Importance of atmospheric inputs and Fe-oxides in controlling soil uranium budgets and behavior along a Hawaiian chronosequence. Chemical Geology, 244(3-4): 691–707.

Pope, G.A., 2013. 4.11 Weathering in the Tropics, and Related Extratropical Processes A2 - Shroder, John F, Treatise on Geomorphology. Academic Press, San Diego, pp. 179-196.

Porder, S., 2014. Coevolution of life and landscapes. Proceedings of the National Academy of Sciences, 111(9): 3207-3208.

Porder, S., Hilley, G.E., 2011. Linking chronosequences with the rest of the world: predicting soil phosphorus content in denuding landscapes. Biogeochemistry, 102(1): 153-166.

Porder, S. et al., 2015. Linking geomorphology, weathering and cation availability in the Luquillo Mountains of Puerto Rico. Geoderma, 249–250: 100-110.

Pourret, O., Davranche, M., Gruau, G., Dia, A., 2007. Competition between humic acid and carbonates for rare earth elements complexation. Journal of Colloid and Interface Science, 305(1): 25-31.

Scatena, F.N., 1989. An introduction to the physiography and history of the Bisley Experimental Watersheds in the Luquillo Mountains of Puerto Rico. USDA Forest Service, General Technical Report SO-72, pp. 22.

Scatena, F.N., Lugo, A.E., 1995. Geomorphology, disturbance, and the soil and vegetation of two subtropical wet steepland watersheds of Puerto Rico. Geomorphology, 13: 199-213.

Schaetzl, R.J., Anderson, S., 2005. Soils Genesis and Geomorphology. Cambridge University Press, New York, 817 pp.

Schoeneberger, P.J., Wysocki, D.A., Benham, E.C., Staff, S.S., 2012. Field book for describing and sampling soils, Version 3.0. Natural Resources Conservation Service, National Soil Survey Center, Lincoln, NE.

Schulz, M.S., White, A.F., 1999. Chemical weathering in a tropical watershed, Luquillo Mountains, Puerto Rico; III. Quartz dissolution rates. Geochimica et Cosmochimica Acta, 63(3-4): 337-350.

Sholkovitz, E.R., 1995. The aquatic chemistry of rare earth elements in river waters. Aquatic Geochemistry, 1: 1-34.

Siebert, C. et al., 2015. Molybdenum isotope fractionation in soils: Influence of redox conditions, organic matter, and atmospheric inputs. Geochimica et Cosmochimica Acta, 162: 1-24.

Silver, W.L., Scatena, F.N., Johnson, A.H., Siccama, T.G., Sanchez, M.J., 1994. Nutrient availability in a montane wet tropical forest: Spatial patterns and methodological considerations. Plant and Soil, 164: 129-145.

Smith, A.L., Schellekens, J.H., Diaz, A.M., 1998. Batholiths as markers of tectonic change in the northeastern Caribbean. Geol. Soc. Am. Spec. Pap. 322, 99-122.

Stallard, R., 2012. Weathering, Landscape Equilibrium, and Carbon in Four Watersheds in Eastern Puerto Rico. In: Murphy, S.F., Stallard, R.F. (Eds.), Water Quality and Landscape Processes of Four Watersheds in Eastern Puerto Rico. Geological Survey Profesional Paper. US Geological Survey, Reston, Virginia, pp. 199-262.

Stone, M.M., Plante, A.F., 2014. Changes in phosphatase kinetics with soil depth across a variable tropical landscape. Soil Biology and Biochemistry, 71(Supplement C): 61-67.

Stonestrom, D.A., White, A.F., Akstin, K.C., 1998. Determining rates of chemical weathering in soils-solute transport versus profile evolution. Journal of Hydrology, 209(1-4): 331-345.

Tebo, B.M., Johnson, H.A., McCarthy, J.K., Templeton, A.S., 2005. Geomicrobiology of 750 manganese (II) oxidation. Trends in Microbiology, 13(9): 421-428.

Teng, F.Z., Li, W.Y., Rudnick, R.L., Gardner, L.R., 2010. Contrasting lithium and magnesium isotope fractionation during continental weathering. Earth and Planetary Science Letters, 300: 63-71.

Thompson, A., Amistadi, M.K., Chadwick, O.A., Chorover, J., 2013. Fractionation of yttrium and holmium during basaltic soil weathering. Geochimica et Cosmochimica Acta, 119: 18-30.

Thompson, A., Chadwick, O.A., Rancourt, D.G., Chorover, J., 2006. Iron-oxide crystallinity increases during soil redox oscillations. Geochimica et Cosmochimica Acta, 70(7): 1710-1727.

Tyler, G., 2004. Rare earth elements in soil and plant systems - A review. Plant Soil, 267(1): 191-206.

Vázquez-Ortega, A. et al., 2016. Solid-phase redistribution of rare earth elements in hillslope pedons subjected to different hydrologic fluxes. Chemical Geology, 426: 1-18.

Vázquez-Ortega, A. et al., 2015. Rare earth elements as reactive tracers of biogeochemical weathering in forested rhyolitic terrain. Chemical Geology, 391: 19-32.

Viers, J., Wasserburg, G.J., 2004. Behavior of Sm and Nd in a lateritic soil profile11Associate editor: G. R. Helz. Geochimica et Cosmochimica Acta, 68(9): 2043-2054.

Viers, J., Dupre, B., Polve, M., Schott, J., Dandurand, J.-L., Braun, J.-J., 1997. Chemical weathering in the drainage basin of a tropical watershed (Nsimi-Zoetele site, Cameroon): comparison between organic-poor and organic-rich waters. Chemical Geology 140, 181-206.

White, A.F. et al., 1998. Chemical weathering in a tropical watershed, Luquillo Mountains, Puerto Rico: I. Long-term versus short-term weathering fluxes. Geochimica et Cosmochimica Acta, 62(2): 209-226.

Yi-Balan, S.A., Amundson, R., Buss, H.L., 2014. Decoupling of sulfur and nitrogen cycling due to biotic processes in a tropical rainforest. Geochimica et Cosmochimica Acta, 142: 411-428.

Yusoff, Z.M., Ngwenya, B.T., Parsons, I., 2013. Mobility and fractionation of REEs during deep weathering of geochemically contrasting granites in a tropical setting, Malaysia. Chemical Geology, 349–350: 71-86.

Ziegler, K., Chadwick, O.A., Brzezinski, M.A., Kelly, E.F., 2005. Natural variations of δ30Si ratios during progressive basalt weathering, Hawaiian Islands. Geochimica et Cosmochimica Acta, 69(19): 4597-4610.

FIGURE CAPTIONS

Figure 1. Location of sampling sites within the Luquillo Critical Zone Observatory in northeastern Puerto Rico. LG1= ridgetop regolith developed over granitic bedrock; B1S1= ridgetop regolith developed over andesitic volcaniclastic bedrock.

Figure 2. Variation of regolith properties with depth in the volcaniclastic (VC) and the granitic regolith profiles. a) Bulk density is generally higher in the granitic regolith, except in the most surficial samples. b) The water content in both profiles is highest near the surface; lowest from 0.9 to 1.2 m depth at the VC site. c) pH is lower in the VC than in the granitic regolith, with peaks at 1.5 and 4.9 m depth in the VC and a gradual increases with depth in the granitic profile. Bulk density in the VC regolith is from Buss et al. (2017) and pH and water content are from Liermann et

al. (2015). Bulk density and pH data in the granitic regolith are from Pett-Ridge et al. (2009b) and water content is from Buss et al. (2005).

Figure 3. Mass transfer coefficient ($\tau_{j,Nb}$) of selected elements in the volcaniclastic (VC) and granitic regolith profiles, using Nb as the index element (Eq. 1). For a given element *j*, $\tau_{j,Nb} > 1$ indicates enrichment, $\tau_{j,Nb} < 1$ indicates depletion and $\tau_{j,Nb} = 0$ indicates no change in mass with respect to the bedrock (vertical lines). a) Relatively immobile elements show non-conservative behavior above 1.8 m depth in the VC profile and are enriched towards the surface in both profiles. b) In the granitic profile, Th shows non-conservative behavior and Zr and Hf are enriched towards the surface of the profile. c) In the VC profile, redox-sensitive elements are lost and gained within a short vertical distance from 1.8 m to the surface of the profile; Mn is strongly enriched at 6.4 m. d) In the granitic profile, Pb and Mn are strongly enriched at 4.3 m depth and Cr at 5.3 m depth. e) In the VC profile, REY are enriched from 4.3 to 6.4 m depth. f) In the granitic regolith, all REY are enriched at 4.3-5.3 m depth, with La also enriched at the surface. Both regolith profiles were sampled until the depth of auger refusal (9.3 m in the VC site, 7.5 m in the granitic site). Unweathered bedrock was sampled at nearby road cuts (granitic) or drill cores (VC); the bedrock depth shown (10 m) for both profiles is arbitrary.

Figure 4. Regolith REE concentrations and our estimation of Saharan dust composition (Table S3), normalized to the local bedrock. a) As weathering proceeds, the VC regolith becomes enriched in all REE until 4.3 m. From 0.6 to 2.7 m depth, the regolith is depleted in MREE and shows a positive Ce anomaly. b) In the granitic regolith, REE are depleted towards the surface and enriched at depth, with an increasing LREE/HREE differentiation from the bottom to the surface of the profile.

Figure 5. Variation of REE ratios with depth in regolith profiles (open symbols), with Saharan dust values for comparison (closed symbols, depth arbitrary). a) LREE/HREE values, represented by $(La/Yb)_N$, increase towards the surface of the granitic profile, but are relatively invariant with depth in the volcaniclastic. b) Fractionation within the LREE group, represented by $(La/Pr)_N$, also increases towards the surface of the granitic profile. c) Fractionation within the HREE group, represented by $(Lu/Ho)_N$, also increases towards the surface of the granitic profile and is highly variable in the upper part of the volcaniclastic regolith. d) Eu anomalies (Eq. 4), trend towards Saharan dust values in the upper half of the granitic profile and a show a decreasing trend with depth in the volcaniclastic profile. The vertical lines indicate bedrock values (i.e., no anomaly for Eu/Eu*). All values are normalized to the local bedrock. Error bars are the propagation of the analytical uncertainty.

Figure 6. Comparison of light (La) and heavy (Yb) REE fractionation, with respect to the MREE (Gd), in a) the volcaniclastic regolith and b) the granitic regolith. The depth of sampling in meters is given beside each symbol. The lines represent the average bedrock values. Arrows represent processes that are known to fractionate REE in a given direction (size arbitrary). The deeper samples in both sites have values close to the bedrock, while the surface samples are enriched in LREE. The most remarkable difference between the two sites is at intermediate depths, where both LREE and HREE are enriched in the volcaniclastic regolith (a) while the granitic regolith shows a gradual enrichment in LREE towards the surface of the profile (b). All values are normalized to the local bedrock. Error bars are the propagation of the of the analytical uncertainty.

Figure 7. Ce anomaly (closed symbols) and average oxygen content (open symbols) variation with depth, representing the long-term and current redox conditions, respectively. a) In the volcaniclastic profile, the Ce anomaly defines an upper, relatively more oxic domain and a less oxic domain below

~4 m depth. The maximum Ce anomaly at 1.8 m depth defines a long-term redox front, at the same depth of the current maximum O_2 content; the Ce anomaly also indicates that redox conditions have been highly variable above 1.5 m depth, including locally reducing or redox-alternating conditions (grey horizontal line). b) In the granitic profile, Ce/Ce* has relatively constant bedrock-like values, except for a positive anomaly at 4.3 m depth. The vertical line is Ce/Ce*=1, i.e., no Ce anomaly. Oxygen data are from Buss et al. (2017).

Figure 8. Summary of relevant properties of the volcaniclastic regolith, from this work and previous studies. At the layer from 0.9 to 1.5 m depth (orange shaded bar), water contents vary the most, bulk density increases (Fig. 2a) and redoximorphic features are most visible. (a) pH is maximum at 1.5 and 4.9 m depth. Major inorganic nutrients (Buss et al., 2017), micro-nutrients (Table 2; Fig. 3c,d) and total bacterial cells (b) reach a minimum within this layer, at ~1 m depth. At the layer from 4.3 to 6.4 m depth (gray shaded bar) heterotrophic cells increase (c), while REY, Mn and other redox-sensitive elements are enriched (d). (e) From 1.5 m depth to the surface (La/Pr)N increases, trending towards dust values; the vertical line indicates the bedrock value. (f) The maximum Ce anomaly marks the depth of a long-term redox front, coincident with the current depth of maximum O2 content (g); the vertical line in Ce/Ce* indicates no anomaly. pH and bacterial total and heterotrophic cells are from Liermann et al. (2015); O2 contents are from Buss et al. (2017).

Table 1. Properties of the volcaniclastic (VC) and granitic regolith profiles

	Volcaniclastic	Granitic	Reference
Lithology	Volcaniclastic, andesitic, marine bedded	Tonalite intrusion (mapped as a quartz diorite)	Briggs and Cortes-Aguilar (1980), Buss et al. (2013)
Elevation[a]	290 masl	672 masl	
Vegetation cover	Mature tabonuco (*Dacryodes excelsa)* forest	Mature palo colorado (*Cyrilla racemiflora*) forest	Scatena and Lugo, 1995
Soil type	Haplomult (US Soil Taxonomy) Ferralsol (WRB)	Plinthic Haplohumult (US Soil Taxonomy) Cambisol (WRB)	Huffaker (2002), Scatena (1989), Silver et al. (1994), Johnson et al. (2011)
Average bedrock mineralogy (wt.%) [b]	Plg = 36%; Chl = 24%; Qz = 10%; Px = 9%; epidote = 8%; K-spar = 6%; Amp = 4%; prehnite = 2%; illite = 1%; calcite = 0.8%; kaolinite = 0.4%	Plg = 56%; Qz = 25%; Bt = 9.5%; Amp = 6.3%; K-spar = 1.8%; goethite = 1.9%.; Chl < 1%; accessory magnetite, sphene, apatite and zircon	Buss et al. (2013, 2017) for the VC bedrock; White et al. (1998) and Pett-Ridge et al. (2009b) for the granitic bedrock
Regolith mineralogy (wt.%) [b, c]	Disordered kaolinite = 30-82%; microcrystalline Qz = 12-29%; halloysite = 9-24%; illite = 7-12%; oxides = 2.5-9% (goethite > gibbsite > hematite); minor Amp, Px and Plg	Plg = 0% above 6 m depth; Qz = 30%, Bt = 18%, kaolinite = 58%; Fe-oxides = 3%	Buss et al. (2017) for the VC regolith; White et al. (1998) for the granitic regolith
Weathering rate	334 ± 46 mm ky^{-1}	45 ± 12 mm ky^{-1}	Dosseto et al. (2012) for the VC site; Chabaux et al. (2013) for the granitic site
Mean annual temperature	22-23 °C	22 °C	Gioda et al. (2013) for the VC site; Stonestrom et al. (1998) for the granitic site
Mean annual precipitation	3678 mm y^{-1}	4050 mm y^{-1}	Gioda et al. (2013) for the VC site; Murphy and Stallard (2012) for the grantic site
Average regolith porosity	0.60 ± 0.08	0.52 ± 0.01	Buss et al. (2017) for the VC site; White et al. (1998) for the granitic site
Infiltration rate	5.0 m y^{-1}	3.2 m y^{-1}	Buss et al. (2017), using data in White et al. (1998) for the granitic site

[a] masl=meters above sea level.

[b] Plg = plagioclase, Qz = quartz, Chl = chlorite, Px = pyroxene, Amp = amphibole, K-spar = potassic feldspar, Bt = biotite. [c] Including soil and saprolite.

Table 2. Elemental concentrations [a] (µg g^{-1}) in regolith and bedrock from the volcaniclastic site

	0 m	0.15 m	0.3 m	0.5 m	0.6 m	0.9 m	1. m	1.2 m	1.5 m	1.8 m	2.7 m	4.3 m	6.4 m	8.2 m	9.3 m	B1W2 1-2	B1W2 1-6	Dust [b]
Bulk density [c] (g cm^{-3})			1.1		1.3	1.3		1.3	1.3	1.2	1.2	1.1	1.2	1.2	1.2	2.3	2.3	
pH [d]	3.9	3.3	3.4	3.3	3.0	3.4	3.4	4.7	4.8	3.7	3.3	3.2	3.7	3.8	3.9			
Li	10.4	8.4	10	9.3	8.1	6	8.3	7.1	6.9	8.3	9	10.1	15	28.5	68.6	13.8	18.2	
Na	138	120	126	107	105	96	100	80	87	124	127	129	155	248	443	9035	12247	5125
Mg	2805	2117	2522	2272	1373	1461	2058	1131	1240	2193	2036	2680	3067	4204	4371	19458	21852	15400
P	318	346	272	280	271	331	323	387	371	266	294	248	301	248	442	445	427	
K	710	725	740	682	410	445	633	490	312	276	816	750	1091	1241	4824	4589	4160	21600
Ca	234	192	107	98	144	146	109	132	136	162	157	201	184	186	192	41034	40314	15650
Sc	35	29	33	35	33	37	37	38	34	35	39	37	40	38	19	18	20	16
Ti	4593	4434	4857	4796	5667	4678	4825	4537	4364	5618	5476	4637	4838	5362	4379	3525	3250	5500
V	189	198	208	212	231	204	209	219	204	200	230	172	201	218	209	202	179	132
Cr	75	89	79	81	59	52	77	101	74	80	78	55	81	71	115	65	48	96
Mn	1095	642	949	617	110	187	490	114	178	241	290	1486	2184	1789	1797	721	631	800
Fe	65920	64814	66123	70207	74537	65488	65085	65640	59010	72401	72761	68125	72444	75306	64349	56630	49969	57000
Co	24	15	20	16	3	2	12	2	2	3	3	20	41	80	79	25	21	18
Ni	42	30	36	43	32	23	41	35	28	28	33	36	49	42	58	36	28	59
Rb	2	2	2	2	2	2	2	2	1	1	2	2	3	4	14	3	4	103
Sr	4	8	3	3	4	2	3	2	2	1	1	1	2	2	17	446	618	208
Y	32.5	16.8	23.9	15	4.4	3	14.7	2.5	3.5	3.9	5.3	26	73.2	30.1	15.2	11.9	12.2	22
Zr	68.4	71.1	68.6	71.1	154.2	100.3	74.1	94.9	105.5	133.7	147.1	108	90.5	114.7	87.4	61.8	60.5	167
Nb	2.2	2.8	2.7	2.9	4.4	2.8	2.8	8.5	2.4	2.4	2.4	2	1.6	2	2.1	1.1	1.3	17
Cs	0.5	0.6	0.7	0.6	0.4	0.3	0.5	0.3	0.2	0.3	0.4	0.4	0.7	0.9	0.8	0.1	0.4	5
Ba	136.3	121.3	139.9	97.1	40.2	31.7	79.6	37.9	37.2	19.1	36.8	124.8	281.1	163.8	452.1	308.1	367	715

La	20.9	24	18.1	12.7	3.1	1.5	11.2	2.8	2.8	1.3	2.4	27.7	28.8	13.8	5.7	8.6	9.4	50
Ce	45	36.8	40.5	28.8	6.2	6.9	25.2	7.3	9.7	10.9	13.9	78.7	47.3	24.4	16.1	21.3	22.5	106
Pr	7.1	6.7	6.7	4.6	0.6	0.4	3.9	0.6	0.6	0.5	0.9	10.3	9.4	4.6	2	3.1	3.5	10
Nd	31.4	26.3	28.9	19.6	2.1	1.6	17	2.1	2.2	1.9	3.8	46.9	41.8	20.6	9.6	14.1	16	49
Sm	6.9	5.5	6.6	4.3	0.5	0.4	3.8	0.4	0.5	0.4	0.7	9.2	10.8	4.8	2.4	3.1	4.7	10
Eu	1.9	1.4	1.8	1.2	0.1	0.1	1	0.1	0.1	0.1	0.2	2	3.2	1.3	0.7	0.8	1.4	2.2
Tb	1	0.6	0.8	0.5	0.1	0.1	0.5	0.1	0.1	0.1	0.1	0.9	1.9	0.7	0.4	0.4	0.6	1.3
Dy	6	3.6	4.9	3.2	0.6	0.5	3	0.5	0.6	0.5	0.8	4.7	11.5	4.6	2.5	2.3	3.3	5
Gd	7	4.5	6.1	3.8	0.4	0.4	3.6	0.4	0.4	0.4	0.6	6.8	11.8	4.8	2.4	2.8	3.7	10
Ho	1.2	0.7	1	0.6	0.1	0.1	0.6	0.1	0.1	0.1	0.2	0.9	2.2	0.9	0.5	0.4	0.7	1.6
Er	3.2	1.9	2.6	1.7	0.5	0.4	1.7	0.3	0.4	0.5	0.7	2.7	5.9	2.5	1.4	1.2	1.9	2
Tm	0.5	0.3	0.4	0.3	0.1	0.1	0.2	0	0.1	0.1	0.1	0.4	0.8	0.4	0.2	0.1	0.4	0.2
Yb	2.6	1.7	2.2	1.5	0.8	0.6	1.4	0.4	0.6	0.6	0.9	2.5	4.9	2.1	1.3	0.9	2	4
Lu	0.4	0.2	0.3	0.2	0.1	0.1	0.2	0.1	0.1	0.1	0.2	0.4	0.7	0.3	0.2	0.1	0.4	0.6
Hf	3.1	3.1	3.1	3.3	4.5	2.9	3.3	2.9	3.1	4	4.1	3.2	2.8	3.4	2.5	1.9	2.9	8
Ta	0.2	0.3	0.3	0.3	0.3	0.2	0.3	0.7	0.2	0.2	0.2	0.2	0.2	0.2	0.2	0.1	0.4	2.5
Pb	6.1	7.1	5.2	6.8	7.3	6.1	6.9	5.9	6.4	3.9	5.1	4.5	4.6	3.9	3.5	2.7	3.6	38
Th	2.2	2.5	2.4	2.7	3.7	2.5	2.7	2.8	2.2	2.5	2.3	1.9	1.7	2	1.1	0.9	1.4	14
U	1.3	1.3	1.3	1.4	1.7	1.3	1.4	1.1	1.2	1.3	1.8	1.4	1	1.2	0.9	0.5	1	3.7

[a] Measurements by ICP-MS at the USGS, Menlo Park, CA. The overall uncertainty is estimated to be better than 4%.

[b] Saharan dust values from Table S3.

[c] Bulk density values from Buss et al. (2017).

[d] pH values from Liermann et al. (2015).

Table 3. Trace element concentrations [a] (µg g^{-1}) in regolith and bedrock from the granitic site

	0.15 m	0.6 m	1.5 m	2.4 m	3.3 m	4.3 m	5.3 m	6.6 m	7.5 m	Bedrock	Dust [b]
Bulk density (g cm^{-3}) [c]	0.7	1.15	1.41	1.32	1.25	1.35	1.4	1.42	1.22	2.7	
pH [c]	4.71	4.58	4.77	4.86	4.67	4.98	5.4	6.21	6.38		
Mg	339	709	1901	1882	2037	1975	3580	5091	5879	6192	15400
Ca	298	123	55	63	217	77	5350	15238	16910	32875	15650
Sc	6	7	16	19	20	17	14	12	13	13	16
Ti	1895	2345	3039	3166	3752	2846	2785	2560	2830	3485	5500
V	92	100	160	149	159	121	114	117	106	154	132
Cr	8	12	8	9	14	6	27	8	7	4	96
Mn	65	129	533	287	439	2533	581	574	599	481	800
Fe	12114	16359	26865	27074	28622	24227	20811	20413	20832	22678	57000
Co	3.3	4.2	15.3	10.2	11.8	29.6	25.3	12.4	12.7	11.7	18
Rb	12	18	45	41	49	43	51	46	50	32	103
Sr	7	5	7	9	7	6	49	143	152	306	208
Y	4	3	14	10	12	15	48	27	34	22	22
Zr	214	123	130	127	103	100	95	96	119	92	167
Nb	3.0	3.4	3.5	3.6	3.9	3.5	3.4	3.1	3.3	2.9	17
Ba	64	113	286	237	306	865	447	528	526	218	715
La	15.5	5.9	10.3	13.4	11.1	11.5	20.3	10.3	9.4	4.0	50
Ce	8.3	10.2	15.1	15.4	16.7	41.9	40.7	16.3	15.1	10.5	106
Pr	1.2	0.7	1.9	2.6	2.0	2.5	6.2	2.4	2.4	1.6	10
Nd	3.1	2.2	6.9	8.8	7.9	9.6	25.3	9.9	10.3	7.4	49
Sm	0.5	0.4	1.5	1.8	1.7	2.2	5.7	2.4	2.5	2.0	10
Eu	0.2	0.1	0.5	0.6	0.6	0.8	1.9	0.8	0.8	0.8	2.2
Gd	0.5	0.4	1.7	1.6	1.7	2.4	6.7	2.8	3.3	2.4	10
Tb	0.1	0.1	0.3	0.3	0.3	0.4	1.2	0.5	0.6	0.4	1.3
Dy	0.5	0.4	1.9	1.6	1.8	2.3	7.5	3.5	4.1	2.7	5

Ho	0.1	0.1	0.4	0.4	0.4	0.5	1.7	0.9	1.0	0.6	1.6
Er	0.4	0.3	1.3	1.0	1.1	1.5	4.9	2.4	2.8	1.7	2
Tm	0.1	0.1	0.2	0.2	0.2	0.3	0.8	0.4	0.5	0.3	0.2
Yb	0.6	0.4	1.6	1.5	1.5	1.9	6.1	2.8	3.0	1.9	4
Lu	0.1	0.1	0.3	0.3	0.3	0.3	1.0	0.5	0.5	0.3	0.6
Hf	4.7	3.1	3.5	3.7	3.0	3.2	3.0	1.8	3.3	2.2	8
Ta	0.1	0.1	0.9	0.2	1.1	0.2	0.2	0.1	0.1	0.1	2.5
Pb	6.2	6.5	6.1	6.0	6.3	13.2	4.5	4.3	4.2	3.5	38
Th	1.6	1.5	3.7	2.4	2.3	1.9	1.8	1.1	1.2	1.1	14
U	1.1	1.0	1.2	1.7	1.7	1.1	0.9	0.4	0.5	0.6	3.7

[a] Measurements by ICP-MS at Cornell University. The overall analytical uncertainty is estimated to be better than 5%.
[b] Saharan dust values from Table S3.
[c] Values from Pett-Ridge et al. (2009b).

Highlights

- We examined trace and rare earth elements during tropical weathering of two bedrocks with similar environmental conditions.

- Trace element mobility has different controls (sorption-desorption or dissolutionprecipitation) depending on the lithology.

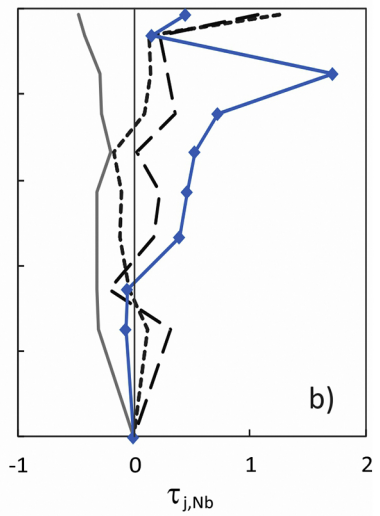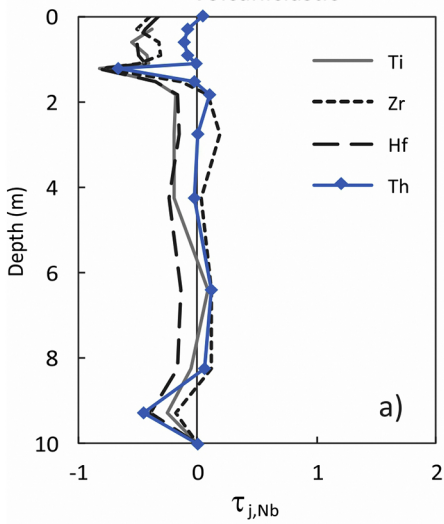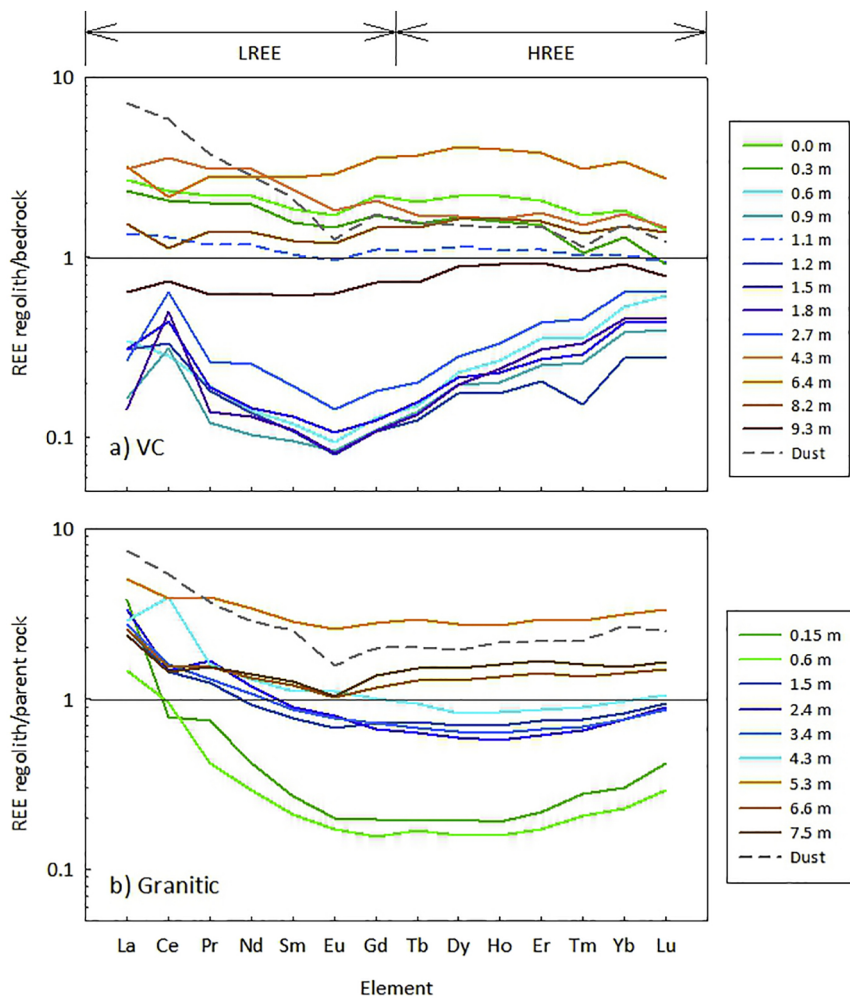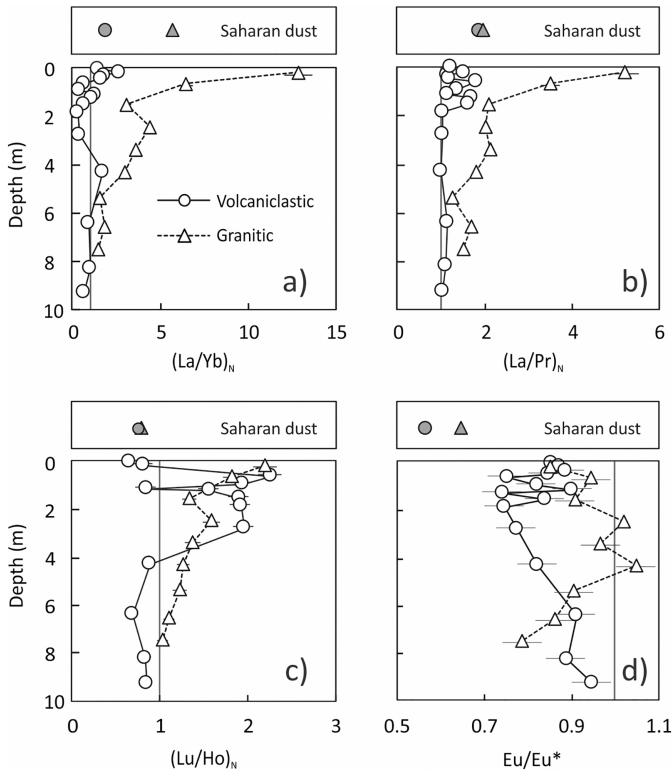- Lithology has a large effect on the long-term redox conditions of the regolith through its effects on texture and mineralogy.
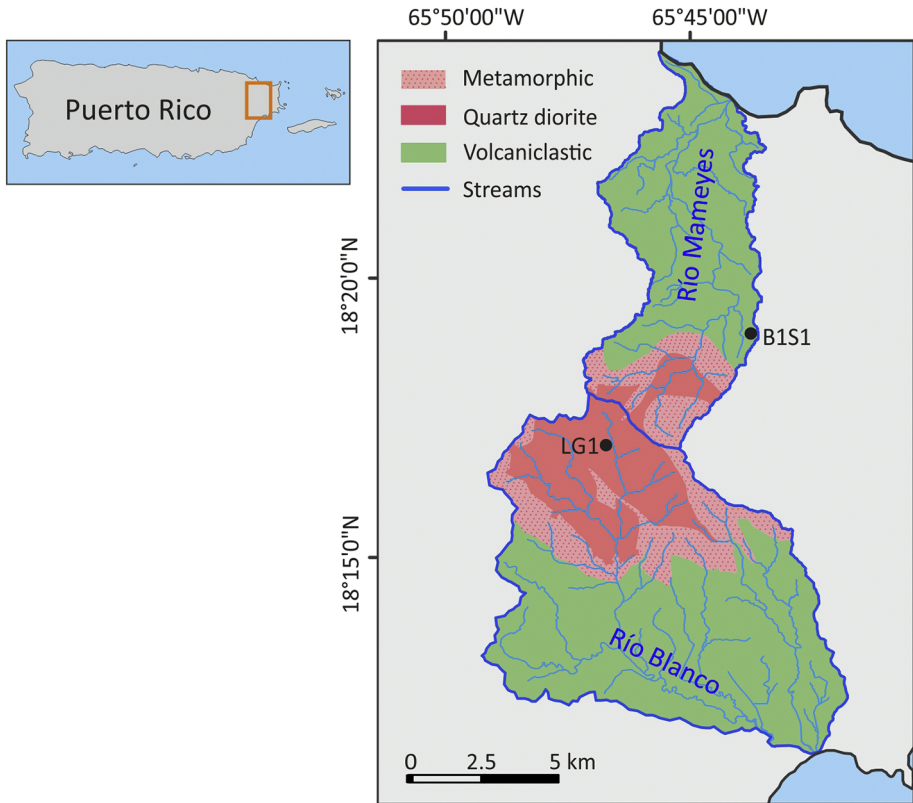
Figure 1
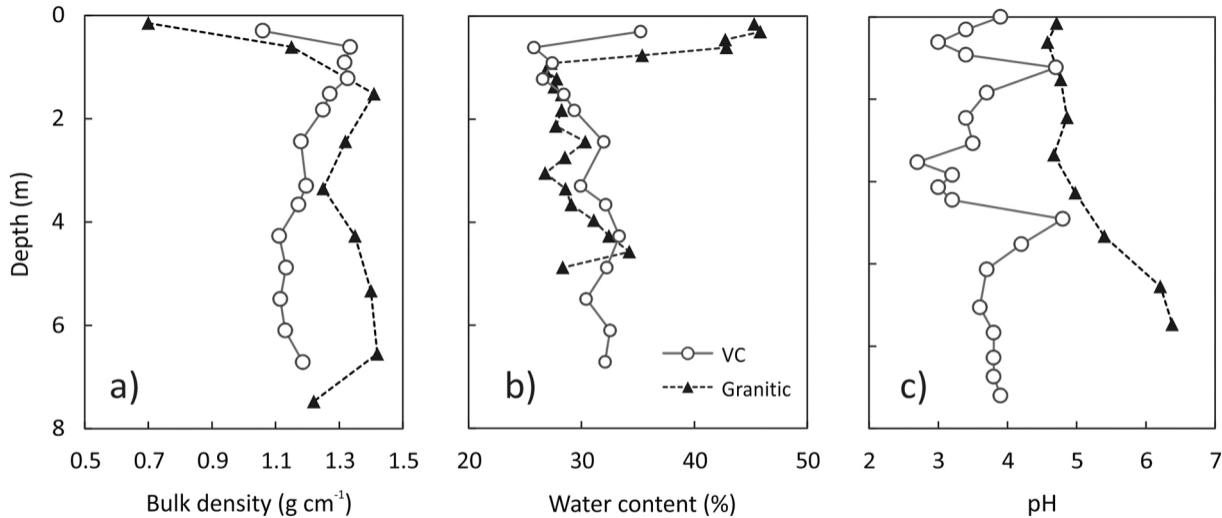
Figure 2
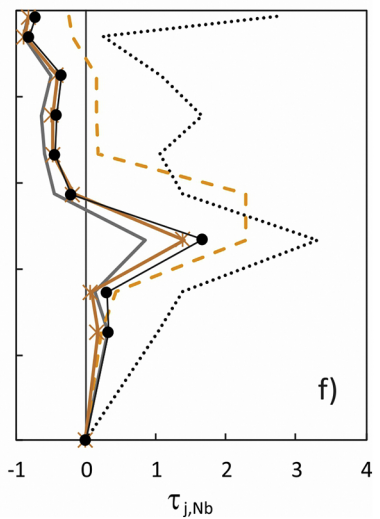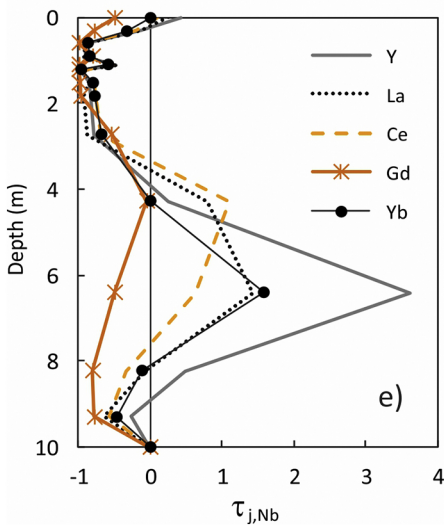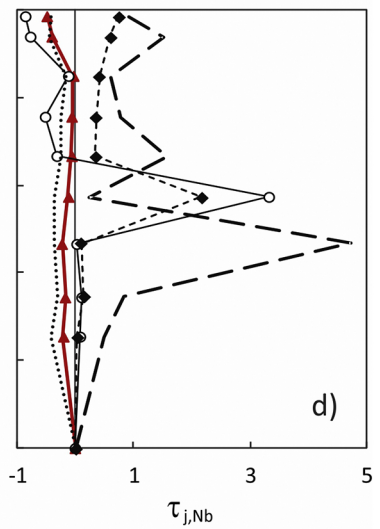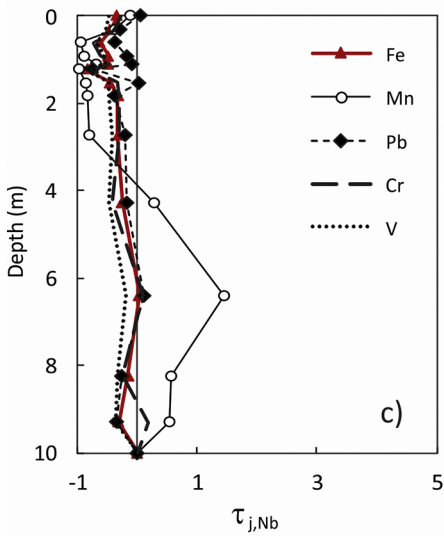
Figure 3

Figure 4

Figure 5

Figure 6

Figure 7

Figure 8